ADVANCES IN ATMOSPHERIC SCIENCES, VOL. 39, APRIL 2022, 625–642

• **Original Paper** •

Influence of the NAO on Wintertime Surface Air Temperature over East Asia: Multidecadal Variability and Decadal Prediction※

Jianping LI*[1,2], Tiejun XIE[3], Xinxin TANG[1], Hao WANG[1], Cheng SUN[3], Juan FENG[3], Fei ZHENG[4], and Ruiqiang DING[5]

[1]*Frontiers Science Center for Deep Ocean Multispheres and Earth System-Key Laboratory of Physical Oceanography-Institute for Advanced Ocean Studies-Academy of the Future Ocean, Ocean University of China, Qingdao* 266100, *China*

[2]*Laboratory for Ocean Dynamics and Climate, Pilot Qingdao National Laboratory for Marine Science and Technology, Qingdao* 266237, *China*

[3]*College of Global Change and Earth System Sciences, Beijing Normal University, Beijing* 100875, *China*

[4]*State Key Laboratory of Numerical Modeling for Atmospheric Sciences and Geophysical Fluid Dynamics, Institute of Atmospheric Physics, Chinese Academy of Sciences, Beijing* 100029, *China*

[5]*State Key Laboratory of Earth Surface Processes and Resource Ecology, Beijing Normal University, Beijing* 100875, *China*

(Received 20 February 2021; revised 28 May 2021; accepted 16 June 2021)

ABSTRACT

In this paper, we investigate the influence of the winter NAO on the multidecadal variability of winter East Asian surface air temperature (EASAT) and EASAT decadal prediction. The observational analysis shows that the winter EASAT and East Asian minimum SAT (EAmSAT) display strong in-phase fluctuations and a significant 60–80-year multidecadal variability, apart from a long-term warming trend. The winter EASAT experienced a decreasing trend in the last two decades, which is consistent with the occurrence of extremely cold events in East Asia winters in recent years. The winter NAO leads the detrended winter EASAT by 12–18 years with the greatest significant positive correlation at the lead time of 15 years. Further analysis shows that ENSO may affect winter EASAT interannual variability, but does not affect the robust lead relationship between the winter NAO and EASAT. We present the coupled oceanic-atmospheric bridge (COAB) mechanism of the NAO influences on winter EASAT multidecadal variability through its accumulated delayed effect of ~15 years on the Atlantic Multidecadal Oscillation (AMO) and Africa–Asia multidecadal teleconnection (AAMT) pattern. An NAO-based linear model for predicting winter decadal EASAT is constructed on the principle of the COAB mechanism, with good hindcast performance. The winter EASAT for 2020–34 is predicted to keep on fluctuating downward until ~2025, implying a high probability of occurrence of extremely cold events in coming winters in East Asia, followed by a sudden turn towards sharp warming. The predicted 2020/21 winter EASAT is almost the same as the 2019/20 winter.

Key words: winter East Asian surface air temperature, North Atlantic Oscillation, Atlantic Multidecadal Oscillation, Africa-Asia multidecadal teleconnection pattern, coupled oceanic-atmospheric bridge, multidecadal variability

Citation: Li, J. P., T. J. Xie, X. X. Tang, H. Wang, C. Sun, J. Feng, F. Zheng, and R. Q. Ding, 2022: Influence of the NAO on wintertime surface air temperature over the East Asia: Multidecadal variability and decadal prediction. *Adv. Atmos. Sci.*, **39**(4), 625–642, https://doi.org/10.1007/s00376-021-1075-1.

Article Highlights:

- Winter EASAT displays a significant 60–80-year multidecadal variability and experienced a decreasing trend in the last two decades.
- The winter NAO leads the detrended winter EASAT by 12–18 years, and the relationship is unaffected by ENSO.
- The coupled oceanic-atmospheric bridge (COAB) mechanism of the NAO influences on winter EASAT multidecadal variability is proposed.
- An NAO-based model predicts the winter EASAT for 2020–34 keeps on fluctuating fall until ~2025 and then turns towards sharp warming.

※ This paper is a contribution to the special issue on Extreme Cold Events from East Asia to North America in Winter 2020/21.

* Corresponding author: Jianping LI
Email: ljp@ouc.edu.cn

1. Introduction

In the first half of winter 2020/21, some extremely cold events occurred over most of China and led to record-breaking cold surface air temperature (SAT) anomalies at many stations during the period (Zheng et al., 2021), which caused serious effects on crops, energy supply, human health, etc. Zheng et al. (2021) pointed out that the synergistic effect of winter 2020/21 La Niña and warm Arctic may have played an important role in the 2020/21 extremely cold winter in China. Zhang et al. (2019) also emphasized the important impacts of equatorial La Niña and mega-La Niña on the cold southern mode (Wang et al., 2010) of winter East Asian SAT (EASAT). Some studies suggested that the Arctic Oscillation (AO)/Northern Hemisphere (NH) Annular Mode (NAM) could contribute to anomalously low SAT in the winter NH mid-latitudes as well as China (Gong et al., 2001; Wu and Wang, 2002; Jeong and Ho, 2005; Li, 2005a, b; Wang and Chen, 2010; Ha et al., 2012; Sun and Li, 2012; Chen et al., 2013; Ding et al., 2014; Yun et al., 2014; Zuo et al., 2015; Li, 2016; Li et al., 2019a) and the springtime extreme low temperature events in northeast China (Yin et al., 2013; Li, 2016). In addition, there are other responsible factors for the winter EASAT, e.g., the autumn and winter Arctic sea ice (Wu et al., 2011a, 2011b; Li and Wu, 2012; Li et al., 2019c; Zhang et al., 2020), autumnal North Pacific sea surface temperature (SST) (Kim and Ahn, 2012), two types of El Niño (Hu et al., 2012), Southern Hemisphere annular mode (SAM) (Wu et al., 2009, 2015; Zheng et al., 2014; Li, 2016), Eurasian snow cover (Yu et al., 2018), etc. These studies mainly focus on the winter EASAT interannual variability. In fact, the winter EASAT and winter East Asian minimum SAT (EAmSAT) time series (Fig. 1) show clear decadal and multidecadal variabilities, which implies that from the perspective of decadal and multidecadal variabilities, one can better understand the variabilities of winter EASAT as well as extremely cold winter events in East Asia and make reasonable decadal predictions for them.

Previous studies have revealed some features of winter EASAT interdecadal variability (Ding et al., 2007, 2014; Wang and Chen, 2014a; Chen et al., 2018; Li et al., 2018a) and multidecadal variability (Gao et al., 2015; Sun et al., 2017a; Li et al., 2019a; Xie et al., 2019). The winter EASAT interdecadal variations seem to be closely associated with major modes of variability in the atmospheric circulation, such as wintertime Ural blocking (Wang and Chen, 2014a), North Atlantic Oscillation (NAO) and NAM/AO (Li et al., 2013a, 2016a, 2018b; Li, 2016; Sun et al., 2017a; Wang et al., 2017; Gong et al., 2019; Xie et al., 2019), Africa–Asia multidecadal teleconnection (AAMT) (Sun et al., 2017a; Li et al., 2019a; Xie et al., 2019), Siberian atmospheric circulation (Ha et al., 2012; Zhao et al., 2014) etc., major modes of variability in the ocean, such as the Atlantic Multidecadal Oscillation (AMO) (Li and Bates, 2007; Li et al., 2013a, 2018b; Luo and Li, 2014; Luo et al., 2017; Sun et al., 2017b), Pacific Decadal Oscillation (PDO) or North Pacific SST (Ding et al., 2014; Luo and Li, 2014; Sun et al., 2016; Xu et al., 2020), combined effect of ENSO and PDO (Kim et al., 2014, 2017), diminishing Arctic sea ice concentration in September (Wang and Chen, 2014a), global SST-forcing (Gao et al., 2015; Xu et al., 2020) etc., and global warming or anthropogenic forcing (Ding et al., 2014; Li et al., 2016a, b, 2018a). Sun et al. (2017a) found that the AAMT is one of the key bridges between cold season EASAT multidecadal variability and the AMO. Xie et al. (2019) further demonstrated that through the AMO and AAMT, the annual EASAT multidecadal variability is closely associated with the annual NAO, and that the former lags the latter by about 15–20 years. However, the manner in which the winter NAO multidecadal variability affects the winter EASAT multidecadal variability and winter extreme temperature events in East Asia still needs to be further investigated, as Li et al. (2019a) mentioned.

Another important question is how to make a decadal prediction for the winter EASAT and extremely cold winters as well. Luo and Li (2014) and Wang and Chen (2014b) employed CMIP5 (Coupled Model Intercomparison Project) models to make a decadal prediction or projections of EASAT. However, climate models have an excessively strong dependence on linear responses to anthropogenic forcing, and as a result they are insufficient for capturing the internal variabilities responsible for the decadal and multi-

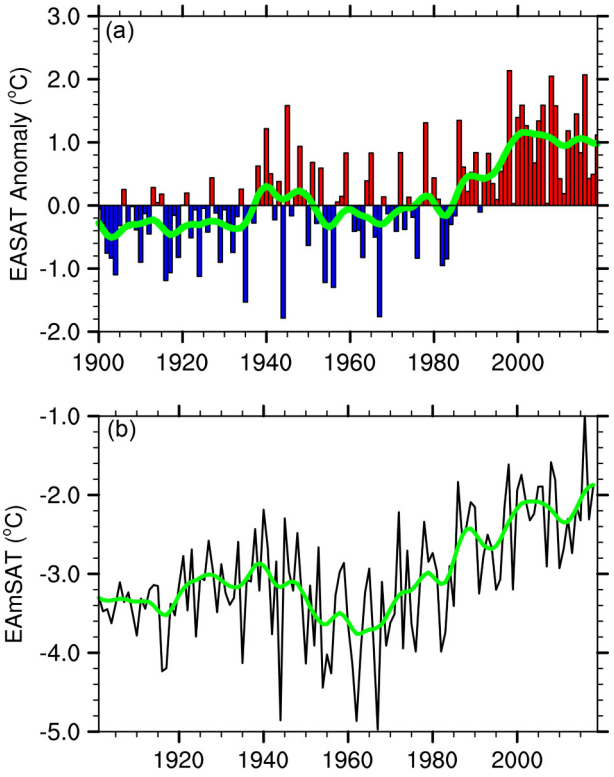

Fig. 1. Winter (DJF) EASAT and EAmSAT time series. (a) Winter EASAT time series (bars) for the period 1900–2019 from a 1961–90 base period based on the HadCRUT4 dataset. The green solid line denotes a 11-year low-pass Gaussian filtered time series. (b) As in (a), but for the winter EAmSAT for 1901–2018 based on the CRU TS4.04 dataset.

decadal variations in SAT. This restricts the capability of decadal and multidecadal prediction of the models (Luo and Li, 2014; Meehl et al., 2014; Meehl and Teng, 2014; Wang et al., 2017; Xing et al., 2017). This implies that developing new approaches for predicting the decadal and multidecadal variations of winter EASAT is needed. Li et al. (2013a) proposed a physics-based empirical prediction model for predicting the decadal variability of the NH mean SAT using the signal that through the oceanic bridge of the AMO the NAO leads the detrended NH mean SAT by 15–20 years. Xie et al. (2019) followed this approach to establish an NAO-based model for decadal prediction of annual EASAT. Here we will further investigate how to construct a physics-based empirical decadal prediction model of winter EASAT and try to explore the future variation of winter EASAT as well as when the cooling trend in the winter EASAT during the past 20 years (see the green line in Fig. 1a) will end.

In this paper we investigate the influence of the winter NAO on the multidecadal variability of winter EASAT and decadal prediction of winter EASAT. Section 2 describes data and methodology. Section 3 analyzes the multidecadal variability of winter EASAT, explores its relation with the winter NAO, and discusses the multidecadal variability of winter EAmSAT and its relation with the winter EASAT. Section 4 studies the relationship between the winter EASAT and ENSO, and explores whether ENSO affects the relationship between the winter NAO and EASAT. Section 5 presents a coupled oceanic-atmospheric bridge (COAB) mechanism on how the winter NAO influences the winter EASAT multidecadal variability. Section 6 constructs a physics-based prediction model of winter decadal EASAT and makes its decadal prediction for 2020–34. Finally, the summary and discussion are given in section 7.

2. Data and methodology

2.1. *Datasets*

The basic information about the gridded datasets employed in this study is summarized in Table 1. These datasets include: the National Center for Atmospheric Research (NCAR) sea level pressure (SLP) observational data (Trenberth and Paolino, 1980) gridded on a 5° × 5° mesh for the period 1899–10/2020, obtained from the US National Center for Environmental Prediction (NCEP); the HadCRUT4 SAT dataset (Morice et al., 2012) on a 5° × 5° grid for the period 1850–2/2020, which is the version 4 of combined land and marine temperature anomalies developed by the Climatic Research Unit (CRU) at the University of East Anglia (UEA) and jointly with the Met Office Hadley Centre, UK; the Twentieth Century Reanalysis Version 2 (20CRv2) data (Compo et al., 2011) on a 2° × 2° grid for the period 1871–2012, obtained from the US National Oceanic and Atmospheric Administration (NOAA); the CRU Time-series (TS) dataset (CRU TS4.04) on a 0.5° × 0.5° grid for the period 1901–2019 (University of East Anglia Climatic Research Unit et al., 2017; Harris et al., 2020), which makes up the some missing data of HadCRUT4 in the central North Africa region; and the Hadley Centre Sea Ice and Sea Surface Temperature dataset (HadISST) on a 1° × 1° grid for the period 1870–2/2020 (Rayner et al., 2003).

2.2. *Indices*

The NAO index (NAOI) is defined as the difference in the normalized, regional zonal-averaged SLP over the North Atlantic (80°W–30°E) between 35°N and 65°N (Li and Wang, 2003), based on the NCAR SLP data (Trenberth and Paolino, 1980). To compare the results from different definitions, another NAOI based on principal component (PC) time series of the leading empirical orthogonal function (EOF) decomposition of SLP anomalies over the Atlantic sector (20°–80°N, 90°W–40°E) (Hurrell, 1995; Hurrell et al., 2003; Hu and Wu, 2004) was also employed. Since the results do not depend on different NAOI definitions, we only display here the results based on the NAOI by Li and Wang (2003). "Winter" here is defined to be the boreal winter, i.e., December–January–February (DJF). For instance, the winter (DJF) 2000/01 is December 2000 and January and February 2001. The winter EASAT time series is defined as the areal-weighted mean DJF SAT anomalies over the studied East Asia domain (20°–40°N, 90°–120°E), relative to the base period 1961–90 and based on the HadCRUT4 dataset (Morice et al., 2012). The winter EAmSAT time series is defined as the areal-weighted mean DJF minimum SAT anomalies over the studied East Asia domain based on the CRU TS4.04 dataset (Harris et al., 2020). The ENSO index is the Niño-3.4 SST index defined as the areal-weighted mean SST anomalies over the Niño-3.4 region (5°N–5°S, 120°–170°W), based on the HadISST data (Rayner et al., 2003). The AMO index and an AMO_c index are respectively defined as the areal-weighted mean SST anomalies over the North Atlantic sector (0°–60°N, 7.5°–75°W) and a

Table 1. Datasets employed in this study.

Variable	Period of record	Spatial resolution	Source
Sea level pressure (SLP)	1899/2020	5° × 5°	NCAR via NCEP (Trenberth and Paolino, 1980)
Surface air temperature (SAT)	1850/2020	5° × 5°	HadCRUT4 via UEA (Morice et al., 2012)
Wind and geopotential height	1871–2012	2° × 2°	20CRv2 data via NOAA (Compo et al., 2011)
Surface climate variables	1901–2019	0.5° × 0.5°	CRU TS4.04 via CRU of UEA (Harris et al., 2020; University of East Anglia Climatic Research Unit et al., 2017)
Sea surface temperature (SST)	1870-2/2020	1° × 1°	HadISST via Met Office Hadley Centre (Rayner et al., 2003)

core region of the North Atlantic (25°–40°N, 20°–50°W) from the HadISST data, with respect to the base period 1961–90 following the removal of the linear trend (e.g., Enfield et al., 2001). The correlation between the two indices is 0.93 on decadal timescale (11-year low-pass Gaussian filtered time series). The AAMT index is the one used by Xie et al. (2019), which is defined by the normalized difference in 300 hPa meridional wind anomalies among the six regions of action of the AAMT based on the 20CRv2 dataset (Compo et al., 2011), instead of the one by Sun et al. (2017a), which is defined by the PC1 time series of the leading EOF of 300 hPa meridional wind anomalies. Since the AAMT has seasonal variation, the six regions of action in winter corresponding to Xie et al. (2019) are A1 [36°–46°N, 50°–40°W], A2 [28°–34°N, 6°W–4°E], A3 [22°–30°N, 24°–32°E], A4 [28°–34°N, 60°–70°E], A5 [20°–26°N, 98°–108°E] and A6 [26°–36°N, 126°–134°E], respectively.

2.3. *Statistical methods*

We applied a two-tailed student *t*-test to test statistical significance. Since variables may have high autocorrelation (e.g., low-pass filtered time series), the number of degrees of freedom is reduced, so the number of effective degrees of freedom, N_{eff}, was used for testing correlation significance. The number of effective degrees of freedom can be theoretically estimated by the following formula (Pyper and Peterman, 1998; Li et al., 2013a, Sun et al., 2019):

$$\frac{1}{N_{\text{eff}}} \approx \frac{1}{N} + \frac{2}{N}\sum_{j=1}^{\infty}\frac{N-j}{N}\rho_{XX}(j)\rho_{YY}(j)\,, \tag{1}$$

where N is the sample size, $\rho_{XX}(j)$ and $\rho_{YY}(j)$ are the autocorrelations of two time series X and Y at lag j, respectively. In practice, one can use the following:

$$\frac{1}{N_{\text{eff}}} \approx \frac{1}{N} + \frac{2}{N}\sum_{j=1}^{N-2}\frac{N-j}{N}\rho_{XX}(j)\rho_{YY}(j)\,. \tag{2}$$

Multiple linear regression was employed to construct a multi-factor regression model. We used the approach by von Storch and Zwiers (2002) to determine the confidence intervals for values simulated or predicted by the multiple linear regression. Like Li et al. (2013a) and Xie et al. (2019, 2021), the multiple linear regression model used for each hindcast was constructed with only the historical data before the hindcast period and a moving hindcast was employed for making complete use of historically observed data with limited length.

Other statistical methods were also employed, for example, detrended analysis, continuous power spectrum analysis, low-pass Gaussian filter, lead–lag correlation analysis, partial correlation and partial regression, composite analysis, and etc.

2.4. *Dynamical diagnosis*

We employed the Rossby wave ray tracing theory in a horizontally non-uniform basic flow (Li and Li, 2012; Li et al., 2015, 2019b; Zhao et al., 2015, 2019) to trace the trajectory of the stationary Rossby wave train and characterize the pathway of the impact of the AAMT. The theory is an extension of the classical one by Hoskins and Karoly (1981). We determined the local group velocity $\boldsymbol{c}_g = \left(u_g, v_g\right)$ as follows

$$u_g = \bar{u}_M + \left[\left(k^2 - l^2\right)\partial\bar{q}/\partial y - 2kl\partial\bar{q}/\partial x\right]/K^4\,, \tag{3a}$$

$$v_g = \bar{v}_M + \left[2kl\partial\bar{q}/\partial y + \left(k^2 - l^2\right)\partial\bar{q}/\partial x\right]/K^4\,, \tag{3b}$$

where $(\bar{u}_M, \bar{u}_M) = (\bar{u}(\lambda,\varphi), \bar{v}(\lambda,\varphi))/\cos\varphi$ is the Mercator projection of the basic states of zonal wind and meridional wind, λ and φ are the longitude and latitude, respectively, k and l are the zonal and meridional wavenumbers, respectively, $K = \sqrt{k^2 + l^2}$ is the total wavenumber, $\bar{q} = 2\Omega\sin\varphi + \nabla^2\overline{\psi}$ is the basic-state absolute vorticity, Ω is the rotation rate of the earth, $\overline{\psi}$ is the basic-state stream function, and

$$\frac{D_g k}{Dt} = -k\frac{\partial\bar{u}_M}{\partial x} - l\frac{\partial\bar{v}_M}{\partial x} + \frac{\partial^2\bar{q}/\partial y\partial x - l\partial^2\bar{q}/\partial x^2}{K^2}\,, \tag{4a}$$

$$\frac{D_g l}{Dt} = -k\frac{\partial\bar{u}_M}{\partial y} - l\frac{\partial\bar{v}_M}{\partial y} + \frac{\partial^2\bar{q}/\partial y^2 - l\partial^2\bar{q}/\partial x\partial y}{K^2}\,, \tag{4b}$$

where $\dfrac{D_g}{Dt} = \dfrac{\partial}{\partial t} + \boldsymbol{c}_g\cdot\nabla_M$ denotes the material derivative moving with the wave ray. The zonal and meridional wavenumbers along a wave ray on a horizontally non-uniform flow are not constant but vary, by contrast with the traditional theory (Hoskins and Karoly, 1981). One can integrate numerically Eqs. (3) and (4) to obtain stationary Rossby wave ray tracing for stationary waves ($\omega = 0$) in a horizontally non-uniform basic flow.

Using the hypsometric equation, the thickness ΔZ of the atmospheric layer between the pressure surfaces p_1 and p_2 is defined as follows (Holton and Hakim, 2013):

$$\Delta Z = Z_2 - Z_1 = \frac{R\langle T\rangle}{g_0}\ln\frac{p_1}{p_2}\,, \tag{5}$$

where Z_1 and Z_2 are the geopotential heights at p_1 and p_2, g_0 =9.80665 m s^{-2} is the global average of gravity at mean sea level, R =287 J kg^{-1} K^{-1} is the gas constant for dry air,

$$\langle T\rangle \equiv \int_{p_2}^{p_1} T d\ln p \Big/ \int_{p_2}^{p_1} d\ln p\,, \tag{6}$$

is the mean temperature of the layer. Thus,

$$\langle T\rangle = \frac{g_0}{R}\left(\ln\frac{p_1}{p_2}\right)^{-1}\Delta Z\,. \tag{7}$$

If let $\langle T\rangle'$ and $\Delta Z'$ be the deviations or anomalies from their time average, then one has the perturbation hypsometric equation as follows:

$$\langle T\rangle' = \frac{g_0}{R}\left(\ln\frac{p_1}{p_2}\right)^{-1}\Delta Z' . \quad (8)$$

Therefore, the perturbation mean temperature of the layer is proportional to the perturbation thickness of a layer bounded by isobaric surfaces. When the perturbation layer thickness thins, the perturbation layer mean temperature falls, and vice versa. We use this perturbation equation of the layer mean temperature to discuss the influences of upper-level atmospheric circulation on tropospheric air temperature anomalies and SAT anomalies.

3. Multidecadal variability in winter EASAT and its relation with NAO

Figure 1 shows the winter (DJF) EASAT and EAmSAT time series. As shown in Fig. 1a, in addition to the long-term warming trend, the winter EASAT has shown obvious characteristics of multidecadal variability since the 1900s. There are two periods of cold winter, 1900–37 and 1952–86. During these periods, wintertime extremely cold events occurred relatively frequently. Although the winter EASAT has experienced a warm phase since 1987, it is significantly different from the global averaged SAT change in that it has shown a decreasing trend for nearly 20 years since the winter EASAT reached the warmest winter in 1998 (Fig. 1a). The winter EAmSAT (1901–2018) also shows similar features (Fig. 1b) and displays strong in-phase fluctuations with the winter EASAT. The correlation coefficients between the raw data of winter EASAT and EAmSAT as well as their 11-year low-pass filtered data are 0.91 and 0.90, respectively, both significant above 99% confidence level using the effective number of degrees of freedom. This suggests that the decreasing trend is conducive to the occurrence of extremely cold events in winter in East Asia. This 20-year warming slowdown of the winter EASAT is significantly longer than that of the global mean SAT (Zuo et al., 2019). Furthermore, at present, there is no evident sign of stopping this cooling trend in the winter EASAT.

The power spectrum results of both the raw and detrended winter EASAT clearly suggest that there is a significant 60–80-year multidecadal variability (Figs. 2a, b). In addition, there are two spectral peaks at ~7 and ~4 years, which are associated with multiyear and interannual variabilities, although they are not significant. These are similar to the spectrum features of the annual EASAT (Xie et al., 2019). The winter EAmSAT also possesses similar spectral characteristics with a significant 60–80-year multidecadal variability (Figs. 2c, d).

Both the annual and seasonal mean NAOI also show significant multidecadal variability with a 60–80-year timescale (Schlesinger and Ramankutty, 1994; Li, 2005a; Delworth et al., 2016; Delworth and Zeng, 2016; Årthun et al., 2017). It can be seen from Fig. 3a that the low frequency components of both the winter NOAI and detrended winter

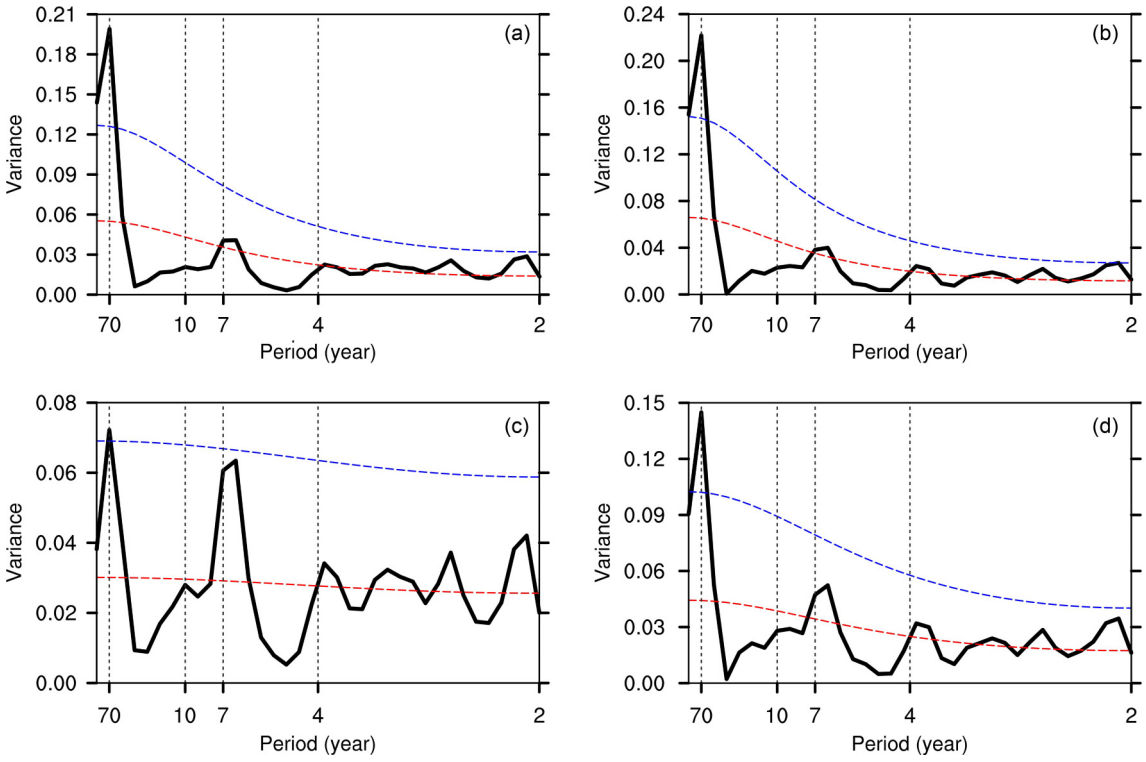

Fig. 2. Power spectrum of winter EASAT and EAmSAT. (a) Power spectrum of the winter EASAT time series (1900–2019). The dashed blue (red) line indicates the 95% confidence level (the reference red noise spectrum). (b) As in (a), but for the winter EAmSAT (1901–2018). (c) As in (a), but for the detrended winter EASAT. (b) As in (d), but for the detrended winter EAmSAT.

EASAT have similar multidecadal variabilities, and the former leads the latter by 10–20 years. The detrended winter EASAT experienced a sharp fluctuating rise from 1980–2000, and has exhibited sharp volatility since then, reaching a relative minimum at the end in the last two decades, which provides a more favorable background condition for the occurrence of winter extremely cold events in East Asia. This is consistent with the results mentioned above. The winter EAmSAT (1901–2018) exhibits similar variations (not shown). The correlation coefficients between the raw data of detrend winter EASAT and EAmSAT as well as their 11-year low-pass filtered data are 0.88 and 0.82, respectively, both significant above 99% and 98% confidence levels using the effective number of degrees of freedom, respectively. The lead–lag correlation analysis (Fig. 3b) between the winter NAOI and detrended winter EASAT for both the unfiltered and low-pass filtered data demonstrates that the winter NAOI leads the detrended winter EASAT by around 12–18 years with the greatest positive correlation (0.72, significant at the 98% confidence level) when the former leads the latter by 15 years, implying the former can account for 52% variance of the latter on an interdecadal timescale.

The correlation map between the detrended winter SAT over East Asia and the winter NAOI 15 years earlier shows a large significantly positive region over East Asia (Fig. 4a), based on 11-year low-pass filtered data and the HadCRUT4 dataset (Morice et al., 2012). A similar result (not shown) was found with the high-resolution dataset of CRU TS4.04 (Harris et al., 2020). The composite difference in SAT (Fig. 4c) also shows this similar pattern. These results show that when the NAO is in a strongly positive phase at multidecadal timescales, SAT anomalies in East Asia are in a warm phase and warm winter becomes more pronounced in East Asia about 15 years later. When the NAO is in a strongly negative phase at multidecadal timescales, there tend to be more cold winters in East Asia about 15 years later. The above results suggest that there is a robust leading relationship between the winter NAOI and detrended EASAT on decadal and multidecadal timescales, implying that the winter NAOI is a potential predictor of decadal and multidecadal variability of the winter EASAT.

4. Winter EASAT and ENSO

In section 3, two spectral peaks at ~7 and ~4 years were found in the winter EASAT, which fall into the principal periods of ENSO. This implies that the winter EASAT might be associated with ENSO. Figure 5 displays the lead–lag correlation between the winter ENSO and EASAT as well as correlation maps between the winter ENSO and SAT over East Asia. As shown in Fig. 5a, the winter ENSO is simultaneously positively correlated with the winter EASAT, but the correlation coefficient is quite small, only 0.20 (significant at the 95% confidence level), which is to say, the winter ENSO can only account for about 4% of the winter EASAT variability. As shown in Fig. 5b, positive correlations between the winter ENSO and SAT are observed in most areas of East Asia. The results imply that on the interannual timescale, ENSO is an influencing factor of winter EASAT, whereby an El Niño event tends to force a warm winter in East Asia and a La Niña tends to have a cold winter more often in East Asia. This is similar to the research of others (Zheng et al., 2021). However, the positive correlations in East Asia are basically smaller than 0.3 (Fig. 5b). This indicates a relatively smaller variance of SAT in East Asia explained by ENSO. In addition, there is no evident correlation between them on interdecadal or multidecadal timescales (Fig. 5a). This implies that although the winter ENSO

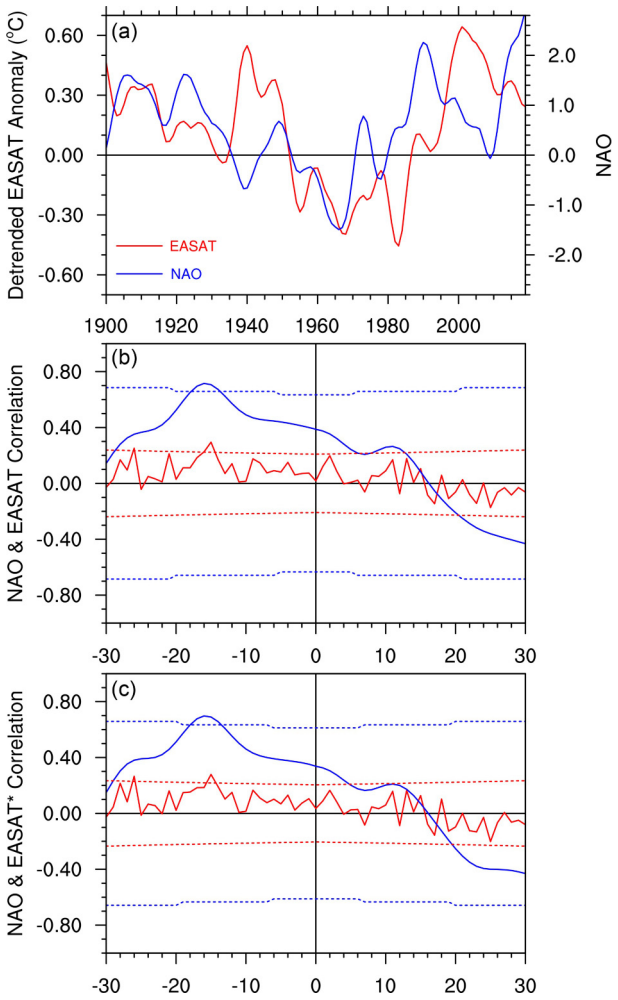

Fig. 3. Winter EASAT, NAOI, and their lead–lag correlation. (a) Winter NAOI (blue) and detrended winter EASAT anomalies (red) and for the period 1900–2019 after 11-year low-pass Gaussian filtering. (b) Lead–lag correlation between the winter NAOI and detrended winter EASAT anomalies (1900–2019). The red (blue) line is for the raw time series (the 11-year low-pass Gaussian filtered). Negative (positive) lags denote that the winter NAOI leads (lags) detrended winter EASAT, and the red (blue) dashed lines indicate the 98% confidence levels for the raw (filtered) time series using the effective number of degrees of freedom. (c) As in (b), but for lead–lag partial correlation in the case when the winter ENSO signal is removed.

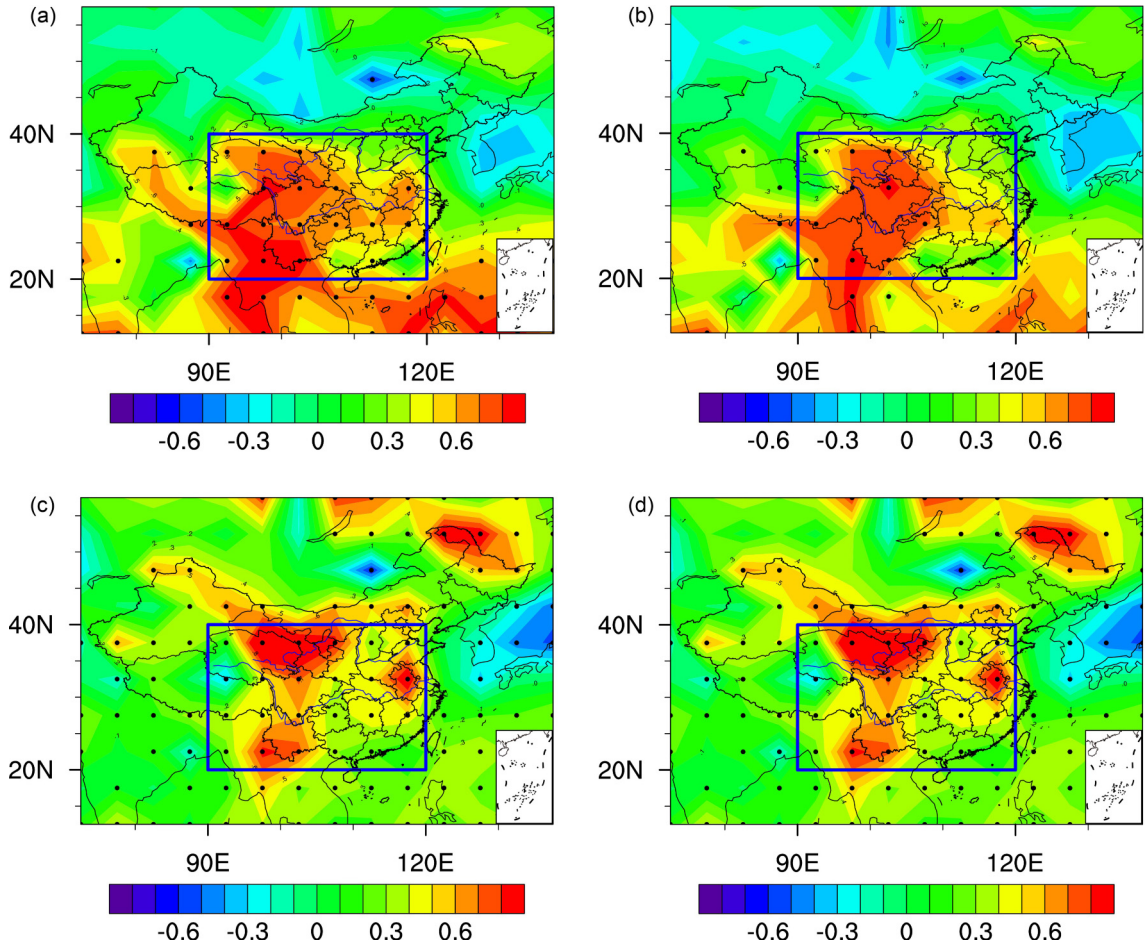

Fig. 4. Lead correlation between winter NAOI and SAT, and composite difference analysis. (a) The lead correlation between the winter NAOI during 1900–2004 and detrended winter SAT over East Asia during 1915–2019 based on the HadCRUT4 dataset and 11-year low-pass Gaussian filtered data. The black dotted area represents significant values at the 95% confidence level using the effective number of degrees of freedom. The blue box denotes the studied East Asian domain (20°–40°N, 90°–120°E). (b) As in (a), but for the case when the winter ENSO signal is removed. (c) As in (a), but for composite difference in detrended winter SAT between the periods 1915–50 and 1995–2019 and the period 1951–85, which lag the positive (1900–35 and 1980–2019) and negative (1936–70) NAO phases by 15 years, respectively. (d) As in (c), but for removing the winter ENSO signal.

may affect the interannual variability of winter EASAT, it may have only a weak influence on the winter EASAT on decadal or multidecadal timescale.

An important question is whether ENSO can affect the robust lead relationship between the winter NAOI and detrended EASAT found in section 2 or not. To clarify this point, partial correlation was employed. After eliminating the winter ENSO signal, we find that the lead–lag correlation between the winter NAOI and detrended winter EASAT (Fig. 3c) is almost the same as the original one (Fig. 3b), and the maximumly leading positive correlation by 15 years is 0.70 (significant at the 98% confidence level). In addition, compared with the original correlation (Fig. 4a) and composite difference (Fig. 4c) patterns, there is not much change in the partial correlation (Fig. 4b) and composite difference (Fig. 4d) maps between the detrended winter SAT over East Asia and the winter NAOI 15 years earlier after removing the winter ENSO signal. By using the high-resolution dataset of CRU TS4.04 we obtain a similar result (not shown) pertaining to the partial correlation map. The results suggest that the robust leading relationship between the winter NAO and EASAT is unaffected by the effect of ENSO. This is consistent with the result by Hu et al. (2011).

5. Coupled oceanic-atmospheric bridge (COAB) mechanism on how NAO influences multidecadal variability in winter EASAT

Li et al. (2013a) shed light on the fact that the NAO influences multidecadal variability of NH mean SAT through its accumulated delayed effect of 15–20 years on the AMO, namely, the AMO plays an oceanic bridge storing NAO information (Li et al., 2019a). Sun et al. (2015) further pro-

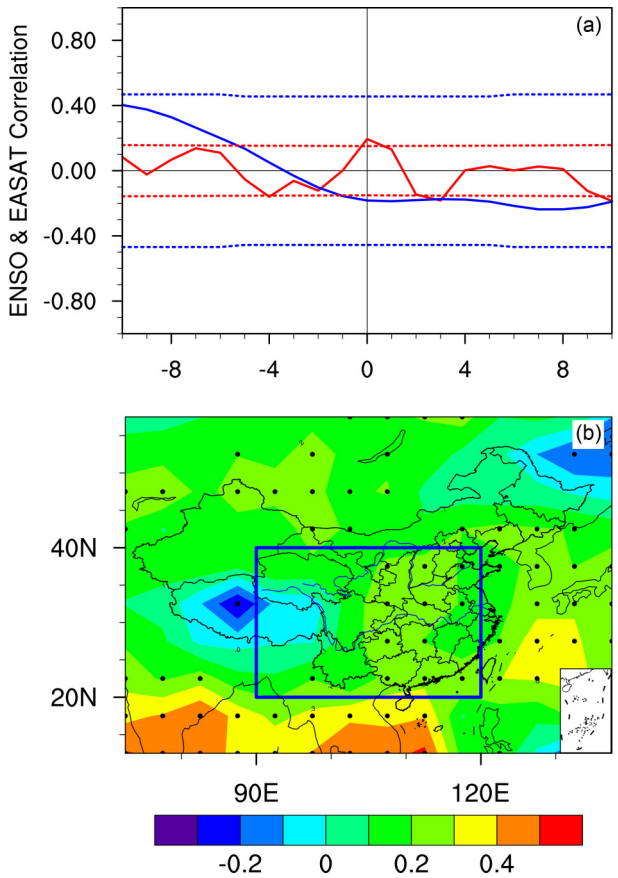

Fig. 5. Correlations between winter ENSO, EASAT and SAT. (a) As in Fig. 3 (b), but for winter ENSO and the 95% confidence levels (dashed lines). (b) Correlation between the winter ENSO and winter SAT (1900–2019). The black dotted area represents significant values at the 95% confidence level using the effective number of degrees of freedom.

posed a delayed oscillator theory to explain the quasi 60-year cycle involved in the multidecadal ocean-atmosphere coupling system in the North Atlantic sector. The positive NAO forces the Atlantic meridional overturning circulation (AMOC) strengthening through an accumulated effect of ~15 years on the AMO and leads to the AMO positive phase, and the AMO in turn provides some negative feedback on the North Atlantic tripole (NAT) and induces the NAO negative phase after ~15 years. Then, the cycle proceeds, but in the opposite sense. Xie et al. (2019) proposed that the annual NAO first stores its signal into the North Atlantic SST anomalies and afterwards impacts annual EASAT on multidecadal timescales via the annual AAMT, which is a key pathway by which the AMO affects EASAT (Sun et al., 2017a). Here we follow these studies and employ the framework of COAB (Li et al., 2013b, 2019a; Li, 2016) to emphasize the COAB mechanism of the winter NAO influences on the multidecadal variability of winter EASAT.

5.1. *AMO as an oceanic bridge storing NAO information*

Figure 6 shows the lead correlation map between the winter NAOI and the SST anomalies over the North Atlantic 15 years later (Fig. 6a) and the partial one after removing the winter ENSO signal (Fig. 6b). The positive correlations between SST anomalies over the North Atlantic and the NAOI 15 years earlier exceed the 95% confidence level, with a basin-wide homogeneous pattern resembling the AMO pattern (Fig. 6a). Slightly different from the annual mean case (Xie et al., 2019), however, the most significant correlations in winter lie in the core region of the North Atlantic (25°–40°N, 20°–50°W), implying that the NAO in winter may mainly exert its accumulated delayed effect on the SST over the core region. The lead–lag correlation between the winter NAOI and AMO_c index shows this link (Fig. 6c), and the largest lead positive correlation of 0.75 (significant at the 98% confidence level) accounts for ~56% variance of the latter on the interdecadal timescale. Moreover, the correlation map (Fig. 6b) and lead–lag correlation (Fig. 6d) remain virtually unchanged after eliminating the winter ENSO signal, and the largest lead partial positive correlation is still 0.75, implying that the robust leading link between the winter NAO and AMO is unaffected by ENSO. The above results suggest that when the winter NAO is in a strong (weak) phase on multidecadal timescales, both winter SST anomalies in the North Atlantic and the winter AMO tend to be in a warm (cold) phase on multidecadal timescales about 15 years later. This is the same finding as reported in previous studies (Li et al., 2013a; Sun et al., 2015; Wills et al., 2019; Xie et al., 2019; Nigam et al., 2020), i.e., the positive (negative) NAO forces the enhancement of the AMOC and in turn leads to the positive (negative) AMO phase with ~15 years delay. Through sustained modulating wind stress anomalies and surface turbulent heat flux anomalies over the core region of the North Atlantic, the NAO can lead to multidecadal fluctuations of the AMOC, which in turn produce the North Atlantic SST signatures of the AMO. The ocean advection process of overturning heat transport associated with the NAO plays a critical role in the AMO evolution. The theoretical time delay, which can be regarded as the time it takes for transport along the overturning heat transport pathway, is ~16 years (Sun et al., 2015).

Figure 7 shows the lead–lag correlation between the winter AMO_c (Fig. 7a) and EASAT and the partial one after removing the winter ENSO signal (Fig. 7b). There is a significant in-phase decadal relation between the winter AMO_c and EASAT. Removing the winter ENSO signal does not change the significant decadal relationship between them (Fig. 7b). The results indicate that when the winter AMO is in a warm (cold) phase on multidecadal timescales, the winter EASAT tends to be in a warm (cold) phase, and thus warm (cold) winter tends to be more often in East Asia on multidecadal timescales. There is substantial observational and modeling evidence that the NAO can lead to multidecadal fluctuations of the AMOC through modulating wind stress anomalies and surface turbulent heat flux anomalies over the North Atlantic (Delworth and Greatbatch,

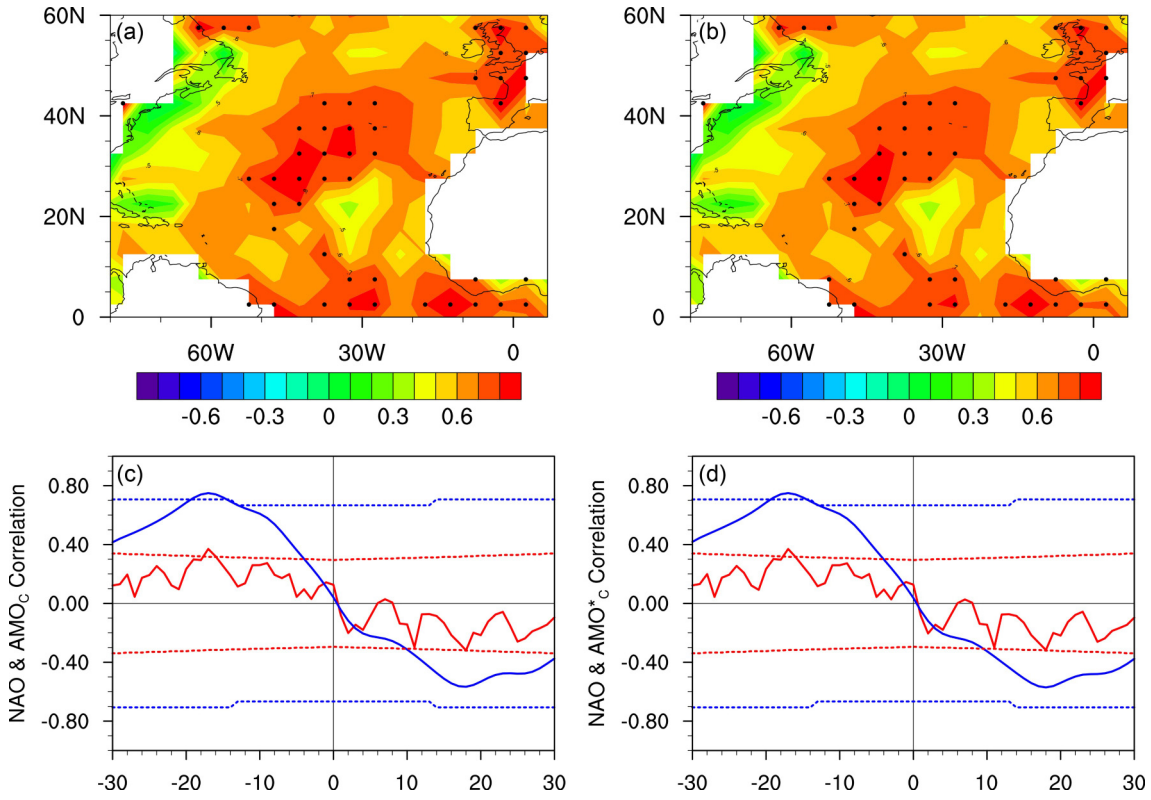

Fig. 6. Lead correlation between winter NAOI and SST. (a) As in Fig. 4a, but for SST anomalies over the North Atlantic. (b) As in (a), but for the case when the winter ENSO signal is removed. (c) As in Fig. 3b, but for the winter NAO and AMO_c. (d) As in (c), but for removing the winter ENSO signal.

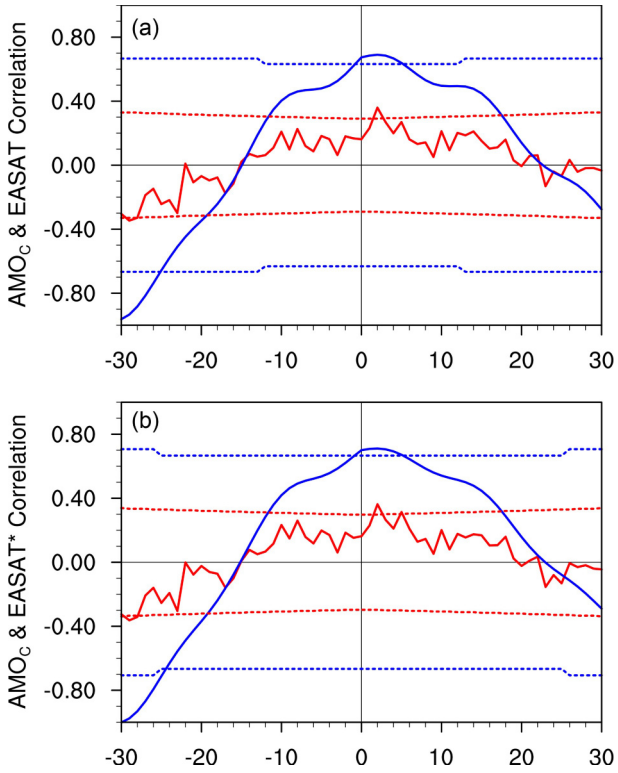

Fig. 7. Lead–lag correlation between winter AMO_c and EASAT. (a) As in Fig. 6 (a), but for the winter EASAT. (b) As in (a), but for the case when the winter ENSO signal is removed.

2000; Latif et al., 2006; Li et al., 2013a; Sun et al., 2015; Stolpe et al., 2018), which in turn produce the North Atlantic SST signatures of the AMO. The relevant dynamics and physical processes are similar with the delayed oscillator theory through the NAO's accumulated delayed effect of 15–20 years proposed in the previous studies for the annual mean case (Li et al., 2013a, 2019a; Sun et al., 2015; Wills et al., 2019; Xie et al., 2019; Nigam et al., 2020), as mentioned above. Therefore, the AMO acts as an oceanic bridge storing NAO information 15 years earlier and connecting the NAO and the EASAT 15 years later on multidecadal timescales.

5.2. *AAMT as an atmospheric bridge conveying the AMO impact onto multidecadal EASAT*

For both cold season and annual mean, Sun et al. (2017a) and Xie et al. (2019) already demonstrated that the AAMT acts as an atmospheric bridge to convey the AMO impact onto multidecadal EASAT. Here we further suggest that this applies to the winter case using the theory of Rossby wave ray tracing in a horizontally nonuniform basic flow and the perturbation hypsometric equation. Figure 8 shows the lead–lag correlation between the winter low-pass filtered AAMT, AMO and EASAT indices. A strong in-phase decadal relationship between the winter AAMT and AMO (Fig. 8a) as well as between the winter AAMT and EASAT (Fig. 8c) is observed. In addition, the significant in-phase decadal relationships between the winter AAMT,

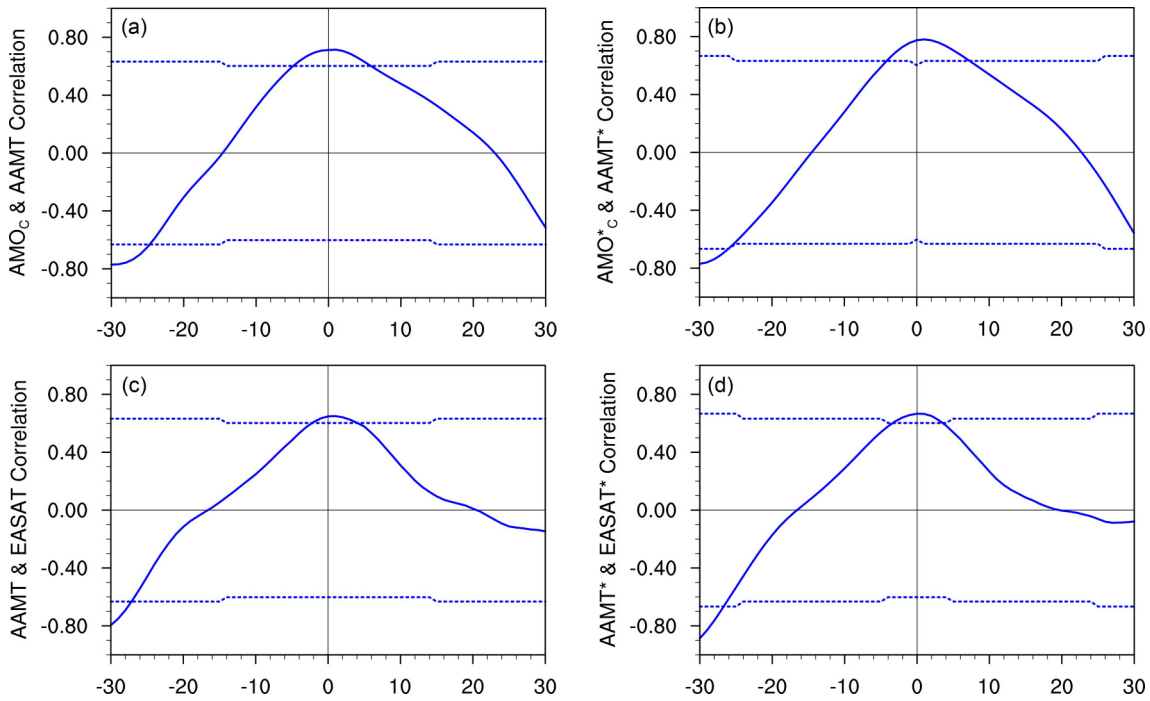

Fig. 8. Lead–lag correlation between winter AAMT, AMO$_c$ and EASAT. (a) As in Fig. 3 (b), but for the winter AAMT and AMO$_c$ indices (1900–2012) using a 11-year Gaussian low-pass filter. (b) As in (a), but for removing winter ENSO signal. (c) As in (a), but for the winter AAMT and EASAT. (d) As in (c), but for removing winter ENSO signal.

AMO and EASAT are not affected greatly by winter ENSO (Figs. 8b and d). That is to say, a positive AAMT phase on multidecadal timescales is corresponding to a warm (cold) AMO phase as well as a warm (cold) EASAT phase on multidecadal timescale, and vice versa. On multidecadal timescales, the AMO may influence SAT in East Asia via the AAMT.

Application of Rossby wave ray tracing in a horizontally nonuniform background flow by Li and Li (2012), Li et al. (2015, 2019b) and Zhao et al. (2015, 2019) was used to produce Fig. 9, which shows the 300 hPa winter stationary Rossby wave trajectories with zonal wavenumbers 5 and 6. These wavenumbers correspond to the zonal scale of the AAMT, starting from the Rossby wave sources over the subtropical region of the south-east North Atlantic. The Rossby wave rays of both zonal wavenumbers 5 and 6 clearly display an eastward propagation along the Africa-Asia subtropical westerly jet, in agreement with the pathway of the AAMT pattern, highlighting the important role of the Africa-Asia subtropical westerly jet in guiding the AAMT wave train from the subtropical North Atlantic to East Asia. The winter AMO can excite the AAMT Rossby wave train to impact the winter EASAT. This is similar to the previous result for the cold season (Sun et al., 2017a).

Upper-level atmospheric circulation could exert strong influences on SAT and tropospheric air temperature through modulating adiabatic expansion and compression of air (Wallace et al., 1996; Sun et al., 2017a). Figure 10 shows the time series of winter detrended tropospheric (300–1000 hPa) mean temperature anomalies over the East Asian domain from the perturbation hypsometric equation. The temperature anomalies estimated by the thickness anomalies between two pressure levels is very consistent with the detrended winter EASAT anomalies in Fig. 3a. The correlation coefficient between the two low-passed timeseries of the estimated winter detrended 300–1000 hPa layer mean temperature anomalies over East Asia and detrended winter EASAT is 0.76, significant above the 99% confidence level. This suggests that the AAMT can modulate tropospheric thickness anomalies over East Asia and in turn cause expansion/compression of the air over East Asia, and consequently lead to the multidecadal variability of EASAT and EAmSAT as well. Thus, the AAMT plays an atmospheric bridge conveying the AMO impact onto the multidecadal variability of EASAT.

6. Physics-based prediction model of winter decadal EASAT and its decadal prediction

Based on the COAB mechanism that the winter NAO influences multidecadal variability in winter EASAT as stated above, we may construct two physics-based models for the winter EASAT. One is an NAO-based linear model for predicting the decadal variability of winter EASAT. Another one is an NAO-ENSO-based linear model which can only be used to fit the winter EASAT variation but cannot be used to make a prediction for the winter EASAT unless the winter ENSO is known in advance. The two models are as follows:

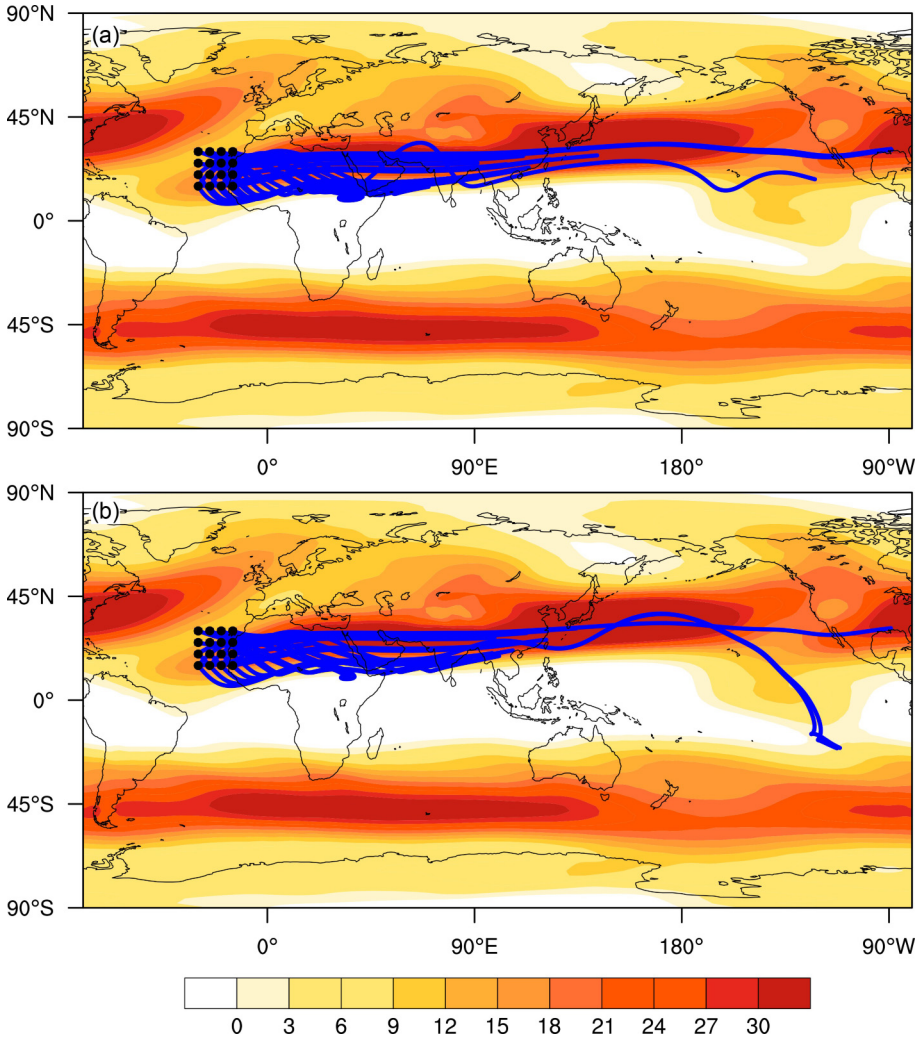

Fig. 9. Stationary Rossby wave trajectories. (a) Winter stationary Rossby wave trajectories in a horizontally nonuniform climatological flow (blue curves) with zonal wavenumber k=5. The black dots denote the Rossby wave source. The shaded area is the climatological mean 300 hPa zonal wind (m s^{-1}). The Rossby wave ray tracing is calculated by adopting the approach by Li and Li (2012), Li et al. (2015) and Zhao et al. (2015). (b) As in (a), but for zonal wavenumber k=6.

$$\widetilde{T_E}(t) = a + b\mathrm{NAO}(t-15) + ct\,, \tag{9}$$

$$\widetilde{T_{E1}}(t) = a_1 + b_1\mathrm{NAO}(t-15) + c_1 t + d_1\mathrm{ENSO}(t)\,, \tag{10}$$

where $\widetilde{T_E}$ and $\widetilde{T_{E1}}$ are the predicts of winter EASAT by the NAO-based model and NAO-ENSO-based model, respectively, t is the time in years, the coefficients a, b, c, a_1, b_1, c_1 and d_1 are determined by the multiple linear regression based on the least square method. The terms ct and $c_1 t$ represent the long-term trend of global warming.

Figure 11 shows the observed and modeled winter decadal EASAT time series for 1915–2019. In the NAO-based decadal prediction model (Fig. 11a), the coefficients a = −29.67, b = 2.48 $\times 10^{-1}$, and c = 1.51 $\times 10^{-2}$. In the NAO-ENSO-based model (Fig. 11b), the coefficients a_1 = −29.67, b_1 = 2.48 $\times 10^{-1}$, c_1 =1.51 $\times 10^{-2}$, and d_1 = −5.37 $\times 10^{-4}$. The modeled winter decadal EASAT of the NAO-based decadal prediction model essentially reproduces the observed one, especially the rapid warming from 1980–2000 and subsequently the decrease in the warming trend over recent years (Fig. 11a). The correlation coefficient between the observed and NAO-based modeled winter decadal EASAT is 0.94, significant at the 99% confidence level. The NAO-ENSO-based model (Fig. 11b) shows almost the same result as the NAO-based model. The correlation coefficient between the observed and NAO-ENSO-based modeled winter decadal EASAT is 0.94, which is virtually the same as the NAO-based model. The corresponding coefficients (a and a_1, b and b_1, c and c_1) of the two models are basically the same. The root mean square errors of the two models are identically 0.18. This is because the coefficient c_1 of winter ENSO is very small. To clarify whether the predictability mostly comes from the linear trend, i.e., if we conduct the same methodology without a linear trend,

the models can still reproduce the decadal and multidecadal variabilities of winter EASAT rather well (Figs. 11c, d). The correlation coefficient between the observed and NAO-ENSO-based modeled winter EASAT without a linear trend are 0.77, almost the same as the NAO-based model. This implies that the significant 60–80-year multidecadal variabilities in both winter NAOI and EASAT (Fig. 2) show high predictability in their low frequency variations, and the robust lead relationship between the winter NAOI and EASAT indicates that the interdecadal EASAT variability can be well predicted by using the winter NAOI. This suggests that the results of the two models have no evident difference even if the additional factor of ENSO is considered in the NAO-ENSO-based model. The result also supports the conclusion mentioned before that the robust lead relationship between the winter NAO and EASAT is unaffected by ENSO. Therefore, the NAO-based model is further discussed in order to make a decadal prediction of winter decadal EASAT.

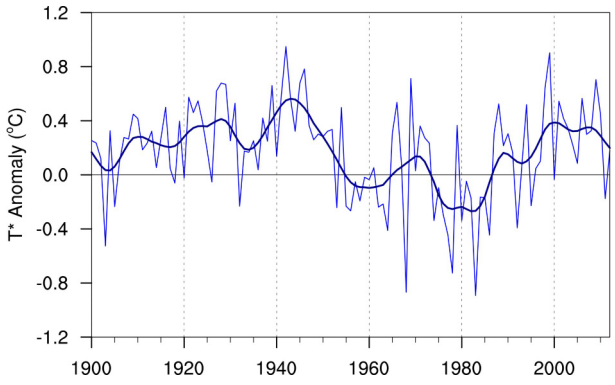

Fig. 10. Time series of winter detrended layer mean temperature anomalies over the East Asian domain. Areal-averaged winter detrended tropospheric (300–1000 hPa) mean temperature anomalies over the studied East Asian domain (blue thin line) estimated by the perturbation hypsometric equation for the period 1900–2012, based on the 20CRv2 dataset and relative to the 1961–90 base period. The solid dark blue line denotes a 11-year low-pass Gaussian filtered time series.

To show the performance of the NAO-based decadal prediction model, figure 12 displays four hindcasted experiments of winter decadal EASAT from the model for four periods 1986–2000 (Fig. 12a), 1991–2005 (Fig. 12b), 1996–2010 (Fig. 12c), and 2001–15 (Fig. 12d). The four hindcasts capture well the sharp fluctuating rise before 2000 (Fig. 12a, b) and the fall after 2000 (Fig. 12c, d) in the observed winter decadal EASAT. Especially, the fluctuating downward after 2005 in the decadal variability of winter EASAT is hindcasted very well. Therefore, the hindcast experiments indicate that on the one hand, the winter NAO is indeed an effective factor for understanding the multidecadal variability of winter EASAT; on the other hand, the NAO-based model can be used to make decadal prediction

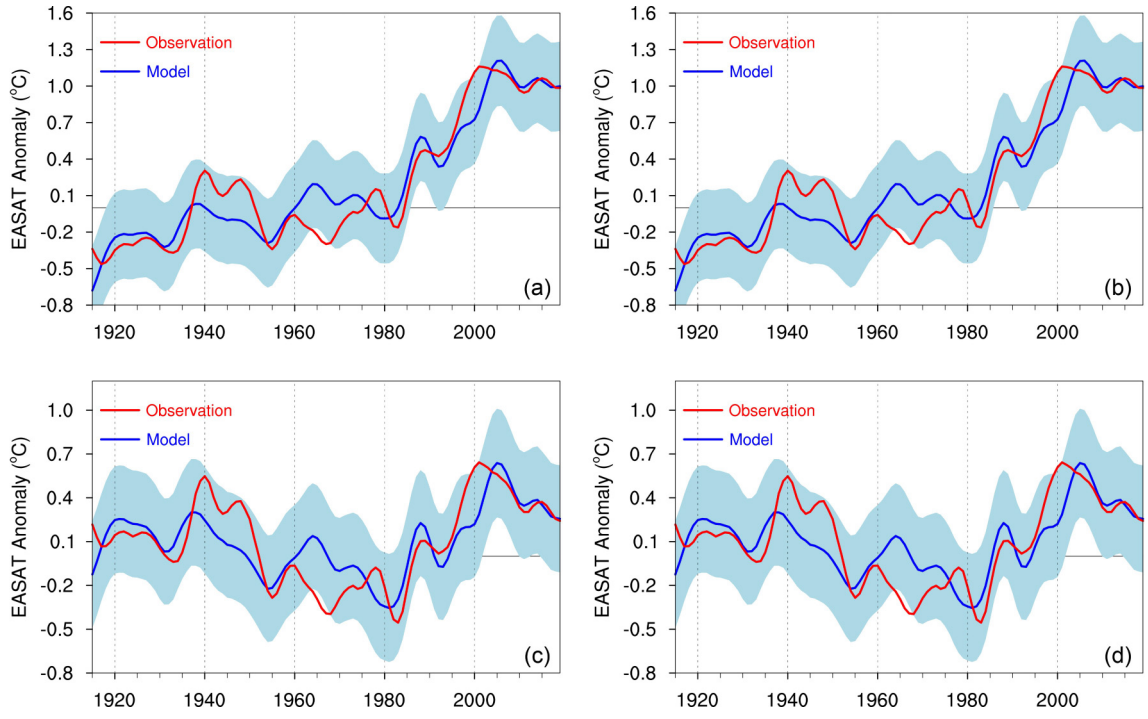

Fig. 11. Observed and modeled winter decadal EASAT. (a) Observed winter decadal EASAT (red) from a 11-year low-pass Gaussian filtering for 1915–2019, and modeled winter decadal EASAT (blue) for 1915–2019 based on the winter NAOI (1900–2004). The model here is the NAO-based decadal prediction model for the winter EASAT. The light blue shaded area indicates the 2-sigma uncertainty range of the modeled values. (b) As in (a), but for the NAO-ENSO-based model and the winter ENSO index (1915–2019). (c) As in (a), but without a linear trend. (d) As in (b), but without a linear trend.

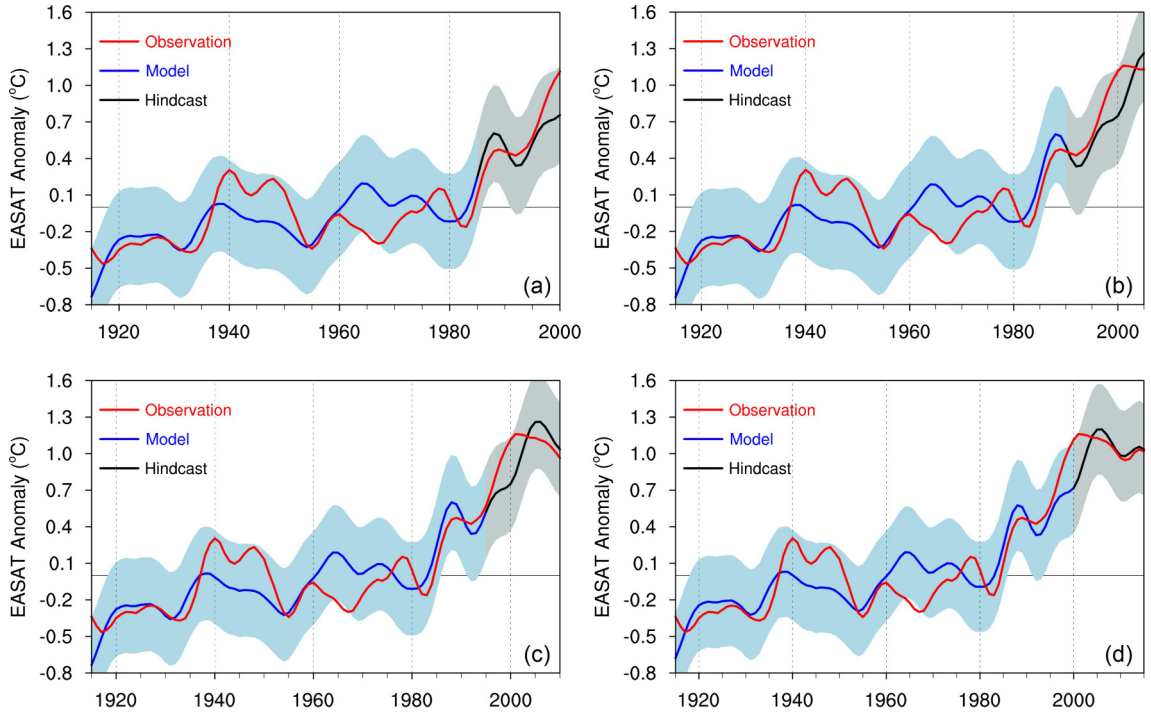

Fig. 12. Observed, modeled, and hindcasted winter decadal EASAT. (a) Observed winter decadal EASAT (red) from 11-year low-pass Gaussian filtering for 1915–2000, modeled winter decadal EASAT (blue) for 1915–1985, and hindcasted winter decadal EASAT (black) for 1986–2000. The model here is the NAO-based decadal prediction model. The shaded areas show the 2-sigma uncertainty range of the modeled and hindcasted values. (b) As in (a), but for observed, modeled and hindcasted winter decadal EASAT for 1915–2005, 1915–90 and 1991–2005, respectively. (c) As in (a), but for observed, modeled and hindcasted winter decadal EASAT for 1915–2010, 1915–95 and 1996–2010, respectively. (d) As in (a), but for observed, modeled and hindcasted winter decadal EASAT for 1915–2015, 1915–2000 and 2001–15, respectively.

for winter EASAT.

We now employ the NAO-based linear model to predict winter decadal EASAT in the next 15 years (2020–34), as shown in Fig. 13. The model is set up by the 1915–2019 historical data. The decadal prediction shows that the winter EASAT will continue fluctuating downward until around 2025 due to the decadal weakening of the previous NAO before around 2010, and afterwards turn towards a sharp warming due to the resonance or synergistic effect of the global warming and recent decadal strengthening of winter NAO. The predicted 2020/21 winter is basically the same as the 2019/20 winter on decadal timescales. The predicted fluctuating downward in winter EASAT until around 2025 implies a high possibility that East Asia will still frequently experience extremely cold winter events over the next few years, since the winter EAmSAT (East Asian minimum SAT) is very highly correlated with the winter EASAT, whether for the raw, low-passed filtering, or detrended time series mentioned above.

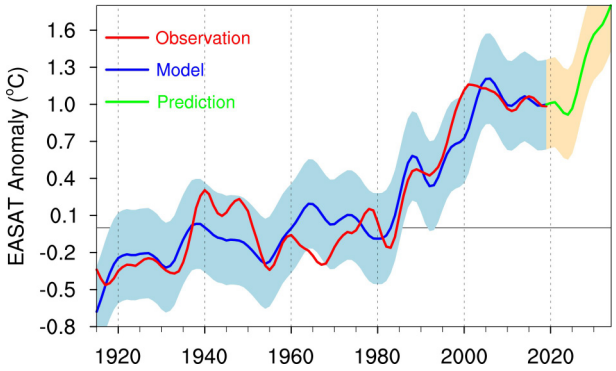

Fig. 13. Observed, modeled, and predicted winter decadal EASAT. Observed winter decadal EASAT (red) after 11-year low-pass Gaussian filtering for 1915–2019, modeled winter decadal EASAT (blue) for 1915–2019, and predicted winter decadal EASAT (green) for 2020–34 based on the NAO-based decadal prediction model. The shaded areas show the 2-sigma uncertainty range of the modeled and predicted values.

7. Summary and discussion

In this paper we have investigated the influence of the winter NAO on the multidecadal variability of winter EASAT and decadal prediction of winter EASAT using the winter NAO. Both the winter EASAT and EAmSAT in the past 120 years were found to display a significant 60–80-year multidecadal variability, apart from a long-term warming trend. There is a strong in-phase relationship between the winter EASAT and EAmSAT. The winter EASAT experienced a decreasing trend over the recent two decades, which is conducive to a greater occurrence of winter extremely

cold events in East Asia in recent years, e.g., extremely cold events in the first half of winter 2020/21 in China. On multidecadal timescales, the winter NAOI leads the detrended winter EASAT by 12–18 years with the strongest significant positive correlation at the lead time of 15 years. When the NAO is in a strongly negative phase on multidecadal timescales, there tends to be more cold winters in East Asia on multidecadal timescale about 15 years later, and vice versa.

Our results imply that ENSO is an influencing factor for the interannual variability of winter EASAT, whereby a La Niña (an El Niño) event tends to force a cold (warm) winter in East Asia, similar to Zheng et al. (2021). However, the winter ENSO can only explain a small portion (~4%) of the variance of the winter EASAT. More importantly, the robust lead relationship between the winter NAO and EASAT is unaffected by ENSO.

We employed the COAB framework (Li, 2016; Li et al., 2013b, 2019a; Liu et al., 2015; Zheng et al., 2015) to present the COAB mechanism of the winter NAO influences on the multidecadal variability of winter EASAT through its accumulated delayed effect of ~15 years on the AMO. The winter AMO acts as an oceanic bridge storing the multidecadal information of winter NAO, the same as the delayed oscillator theory to explain the quasi 60-year cycle involved in the multidecadal ocean-atmosphere coupling system in the North Atlantic sector (Sun et al., 2015; Xie et al., 2019). Employing the theory of Rossby wave ray tracing in a horizontally nonuniform basic flow and the perturbation hypsometric equation, it was shown that the winter AAMT acts as an atmospheric bridge conveying the winter AMO impact onto the multidecadal variability of winter EASAT, similar to Sun et al. (2017a) and Xie et al. (2019) for the cases of the cold season and annual mean, respectively. This demonstrates that the chain process of COAB, the NAO–AMO–AAMT–EASAT, is a vital path by which the NAO influences the multidecadal variability of EASAT.

In the light of the COAB mechanism mentioned above, we constructed two physics-based models, an NAO-based linear model for predicting winter decadal EASAT and an NAO-ENSO-based linear model for fitting the winter EASAT. Our results show that the model performance is virtually unimproved by including the ENSO factor, supporting the other finding that ENSO does not change the relationship between the winter NAO and EASAT. Therefore, the simpler NAO-based decadal prediction model was adopted to predict the decadal variability of winter EASAT. Hindcast experiments demonstrate that the model captured well the observed winter decadal EASAT, including the sharp fluctuating warming before 2000, and the fall after 2000 in the winter decadal EASAT, implying a good decadal prediction performance of the model.

The decadal prediction of the NAO-based model for the next 15 years (2020–34) shows that the winter EASAT will keep fluctuating downward until around 2025, implying a high probability of occurrence of extremely cold events in East Asia in coming winters, and then turn towards a sharp warming. The predicted 2020/21 winter is almost the same as the 2019/20 winter. This may provide a climatological background for the extremely cold events in the past first half of winter 2020/21 in East Asia. The interannual variability of winter EASAT is also associated with the winter ENSO, although the latter has very little influence on the winter EASAT on decadal or multidecadal timescales. Thus, the 2020/21 La Niña event also contributes to 2020/21 winter extremely cold events in East Asia (Zheng et al., 2021).

The observational analysis indicates that at present there is no obvious sign that the cooling trend in the winter EASAT during the past 20 years will end soon. The prediction of the NAO-based model mentioned above also supports this, since the NAO ended its multidecadal decline around 2010. The prediction implies a high possibility that East Asia will still frequently experience extremely cold winter events for the next several years.

In the longer term, the predicted accelerated warming in the winter EASAT after 2025 hints that winters in East Asia will be getting warmer and warmer, and will become the norm. This is due to the synergistic effect of the decadal strengthening of winter NAO after 2010 and the global warming.

It should be pointed out that due to data constraints the lengths of the datasets used are not very long to discuss the multidecadal variabilities of 60–80 years. We may need to wait for longer datasets to further validate the robustness and significance of the results in the future. Also, the AMO displays multiple time scales and is associated with different physical processes. For instance, recently Li et al. (2020) noted that the interannual variation is mainly a lagged response to ENSO through the atmospheric bridge and NAO plays a secondary role, implying at the subannual time scale, both ENSO and NAO may play a role. There is no denying that except for the winter NAO there are other responsible factors for the decadal and multidecadal variabilities of winter EASAT such as other decadal and multidecadal signals in the climate system, warm Arctic, Arctic sea ice, aerosols, volcanic activities, solar activity, etc. Comprehensive research on the integrating influences of these factors on the winter EASAT will be helpful for improving the skill of decadal and multidecadal prediction for the winter EASAT and extremely cold winter events in East Asia.

Acknowledgements. This work was jointly supported by the National Natural Science Foundation of China (NSFC) Project (Grant No. 41790474), Shandong Natural Science Foundation Project (Grant No. ZR2019ZD12), and Fundamental Research Funds for the Central Universities (Grant No. 201962009). The authors wish to thank the support from Center for High Performance Computing and System Simulation, Pilot National Laboratory for Marine Science and Technology (Qingdao), and all data providers.

REFERENCES

Årthun, M., T. Eldevik, E. Viste, H. Drange, T. Furevik, H. L. Johnson, and N. S. Keenlyside, 2017: Skillful prediction of northern climate provided by the ocean. *Nature Communications*, **8**, 15875, https://doi.org/10.1038/ncomms15875.

Chen, J. W., Y. Deng, W. S. Lin, and S. Yang, 2018: A process-based decomposition of decadal-scale surface temperature evolutions over East Asia. *Climate Dyn.*, **51**, 4371–4383, https://doi.org/10.1007/s00382-017-3872-x.

Chen, W., X. Q. Lan, L. Wang, and Y. Ma, 2013: The combined effects of the ENSO and the Arctic Oscillation on the winter climate anomalies in East Asia. *Chinese Science Bulletin*, **58**(12), 1355–1362, https://doi.org/10.1007/s11434-012-5654-5.

Compo, G. P., and Coauthors, 2011: The twentieth century reanalysis project. *Quart. J. Roy. Meteor. Soc.*, **137**, 1–28, https://doi.org/10.1002/qj.776.

Delworth, T. L., and R. J. Greatbatch, 2000: Multidecadal thermohaline circulation variability driven by atmospheric surface flux forcing. *J. Climate*, **13**, 1481–1495, https://doi.org/10.1175/1520-0442(2000)013<1481:MTCVDB>2.0.CO;2.

Delworth, T. L., and F. R. Zeng, 2016: The impact of the North Atlantic Oscillation on climate through its influence on the Atlantic Meridional Overturning Circulation. *J. Climate*, **29**, 941–962, https://doi.org/10.1175/JCLI-D-15-0396.1.

Delworth, T. L., F. R. Zeng, G. A. Vecchi, X. S. Yang, L. P. Zhang, and R. Zhang, 2016: The North Atlantic Oscillation as a driver of rapid climate change in the Northern Hemisphere. *Nature Geoscience*, **9**, 509–512, https://doi.org/10.1038/ngeo2738.

Ding, Y. H., and Coauthors, 2007: China's national assessment report on climate change (I): Climate change in China and the future trend. *Advances in Climate Change Research*, **3**, 1–5.

Ding, Y. H., and Coauthors, 2014: Interdecadal variability of the East Asian winter monsoon and its possible links to global climate change. *J. Meteor. Res.*, **28**(5), 693–713, https://doi.org/10.1007/s13351-014-4046-y.

Enfield, D. B., A. M. Mestas-Nuñez, and P. J. Trimble, 2001: The Atlantic Multidecadal Oscillation and its relation to rainfall and river flows in the continental U.S. *Geophys. Res. Lett.*, **28**, 2077–2080, https://doi.org/10.1029/2000GL012745.

Gao, L. H., Z. W. Yan, and X. W. Quan, 2015: Observed and SST-forced multidecadal variability in global land surface air temperature. *Climate Dyn.*, **44**, 359–369, https://doi.org/10.1007/s00382-014-2121-9.

Gong, D. Y., S. W. Wang, and J. H. Zhu, 2001: East Asian winter monsoon and Arctic Oscillation. *Geophys. Res. Lett.*, **28**, 2073–2076, https://doi.org/10.1029/2000GL012311.

Gong, H. N., L. Wang, and W. Chen, 2019: Multidecadal changes in the influence of the Arctic Oscillation on the East Asian surface air temperature in boreal winter. *Atmosphere*, **10**, 757, https://doi.org/10.3390/atmos10120757.

Ha, K.-J., K.-Y. Heo, S.-S. Lee, K.-S. Yun, and J.-G. Jhun, 2012: Variability in the East Asian monsoon: A review. *Meteorological Applications*, **19**(2), 200–215, https://doi.org/10.1002/met.1320.

Harris, I., T. J. Osborn, P. Jones, and D. Lister, 2020: Version 4 of the CRU TS monthly high-resolution gridded multivariate climate dataset. *Scientific Data*, **7**, 109, https://doi.org/10.1038/s41597-020-0453-3.

Holton, J. R., and G. J. Hakim, 2013: *An Introduction to Dynamic Meteorology*. 5th ed. Academic Press, 552 pp, https://doi.org/10.1016/C2009-0-63394-8.

Hoskins, B. J., and D. J. Karoly, 1981: The steady linear response of a spherical atmosphere to thermal and orographic forcing. *J. Atmos. Sci.*, **38**(6), 1179–1196, https://doi.org/10.1175/1520-0469(1981)038<1179:TSLROA>2.0.CO;2.

Hu, Z. Z., and Z. H. Wu, 2004: The intensification and shift of the annual North Atlantic Oscillation in a global warming scenario simulation. *Tellus A*, **56**, 112–124, https://doi.org/10.1111/j.1600-0870.2004.00050.x.

Hu, Z. Z., A. Kumar, B. H. Huang, Y. Xue, W. Q. Wang, and B. Jha, 2011: Persistent atmospheric and oceanic anomalies in the North Atlantic from Summer 2009 to Summer 2010. *J. Climate*, **24**(22), 5812–5830, https://doi.org/10.1175/2011JCLI4213.1.

Hu, Z. Z., A. Kumar, B. Jha, W. Q. Wang, B. H. Huang, and B. Y. Huang, 2012: An analysis of warm pool and cold tongue El Niños: Air–sea coupling processes, global influences, and recent trends. *Climate Dyn.*, **38**, 2017–2035, https://doi.org/10.1007/s00382-011-1224-9.

Hurrell, J. W., 1995: Decadal trends in the North Atlantic Oscillation: Regional temperatures and precipitation. *Science*, **269**, 676–679, https://doi.org/10.1126/science.269.5224.676.

Hurrell, J. W., Y. Kushnir, G. Ottersen, and M. Visbeck, 2003: An overview of the North Atlantic oscillation. *The North Atlantic Oscillation: Climatic Significance and Environmental Impact*, J. W. Hurrell et al., Eds., AGU, **134**, 1–35, https://doi.org/10.1029/134GM01.

Jeong, J. H., and C. H. Ho, 2005: Changes in occurrence of cold surges over East Asia in association with Arctic Oscillation. *Geophys. Res. Lett.*, **32**, 85–93, https://doi.org/10.1029/2005GL023024.

Kim, H. J., and J. B. Ahn, 2012: Possible impact of the autumnal North Pacific SST and November AO on the East Asian winter temperature. *J. Geophys. Res.*, **117**, D12104, https://doi.org/10.1029/2012JD017527.

Kim, J.-W., S.-W. Yeh, and E.-C. Chang, 2014: Combined effect of El Niño-Southern Oscillation and Pacific decadal oscillation on the East Asian winter monsoon. *Climate Dyn.*, **42**(3–4), 957–971, https://doi.org/10.1007/s00382-013-1730-z.

Kim, J.-W., S.-I., An, S.-Y. Jun, H.-J. Park, and S. W. Yeh, 2017: ENSO and East Asian winter monsoon relationship modulation associated with the anomalous northwest Pacific anticyc-

lone. *Climate Dyn.*, **49**(4), 1157–1179, https://doi.org/10.1007/s00382-016-3371-5.

Latif, M., C. Boning, J. Willebrand, A. Biastoch, J. Dengg, N. Keenlyside, U. Schweckendiek, and G. Madec, 2006: Is the thermohaline circulation changing? *J. Clim.*, **19**(18), 4631–4637.

Li, C. X., T. B. Zhao, and K. R. Ying, 2016b: Effects of anthropogenic aerosols on temperature changes in China during the twentieth century based on CMIP5 models. *Theor. Appl. Climatol.*, **125**, 529–540, https://doi.org/10.1007/s00704-015-1527-6.

Li, J. P., 2005a: Coupled air-sea oscillations and climate variations in China. *Climate and Environmental Evolution in China (First Volume)*, D. H. Qin, Ed., China Meteorological Press, 324–333. (in Chinese)

Li, J. P., 2005b: Physical nature of the Arctic Oscillation and its relationship with East Asian atmospheric circulation. *Air-Sea Interaction and its impacts on China Climate*, Y. Q. Yu and W. Chen, Eds., China Meteorological Press, 169–176. (in Chinese)

Li, J. P., 2016: Impacts of annular modes on extreme climate events over the East Asian monsoon region. *Dynamics and Predictability of Large-Scale, High-Impact Weather and Climate Events*, J. P. Li et al., Eds., Cambridge University Press, 343–353, https://doi.org/10.1017/CBO9781107775541.028.

Li, J. P., and J. X. L. Wang, 2003: A new North Atlantic Oscillation index and its variability. *Adv. Atmos. Sci.*, **20**, 661–676, https://doi.org/10.1007/BF02915394.

Li, J. P., and Z. W. Wu., 2012: Importance of autumn Arctic sea ice to northern winter snowfall. *Proceedings of the National Academy of Sciences of the United States of America*, **109**, E1898, https://doi.org/10.1073/pnas.1205075109.

Li, J. P., C. Sun, and F.-F. Jin, 2013a: NAO implicated as a predictor of Northern Hemisphere mean temperature multidecadal variability. *Geophys. Res. Lett.*, **40**, 5497–5502, https://doi.org/10.1002/2013GL057877.

Li, J. P., C. Sun, and R. Q. Ding, 2018b: A coupled decadal-scale air-sea interaction theory: The NAO-AMO-AMOC coupled mode and its impacts. *Global Change and Future Earth-The Geoscience Perspective*, T. Beer et al., Eds., Cambridge University Press, 131–143.

Li, J. P., R. Swinbank, R. Grotjahn, and H. Volkert, 2016a: *Dynamics and Predictability of Large-Scale, High-Impact Weather and Climate Events*. Cambridge University Press, 370pp.

Li, J. P., F. Zheng, C. Sun, J. Feng, and J. Wang, 2019a: Pathways of influence of the Northern Hemisphere mid–high latitudes on East Asian climate: A review. *Adv. Atmos. Sci.*, **36**, 902–921, https://doi.org/10.1007/s00376-019-8236-5.

Li, J. P., H. H. Hsu, W. C. Wang, K. J. Ha, T. M. Li, and A. Kitoh, 2018a: East Asian climate under global warming: Understanding and projection. *Climate Dyn.*, **51**, 3969–3972, https://doi.org/10.1007/s00382-018-4523-6.

Li, J. P., and Coauthors, 2013b: Progress in air–land–sea interactions in Asia and their role in global and Asian climate change. *Chinese Journal of Atmospheric Sciences*, **37**, 518–538, https://doi.org/10.3878/j.issn.1006-9895.2012.12322. (in Chinese with English abstract)

Li, S. L., and G. T. Bates, 2007: Influence of the Atlantic multidecadal oscillation on the winter climate of East China. *Adv. Atmos. Sci.*, **24**, 126–135, https://doi.org/10.1007/s00376-007-0126-6.

Li, X. F., Z. Z. Hu, and B. H. Huang, 2020: Subannual to interannual variabilities of SST in the North Atlantic Ocean. *J. Climate*, **33**(13), 5547–5564, https://doi.org/10.1175/JCLI-D-19-0556.1.

Li, X. X., Z. W. Wu, and Y. J. Li, 2019c: A link of China warming hiatus with the winter sea ice loss in Barents–Kara Seas. *Climate Dyn.*, **53**, 2625–2642, https://doi.org/10.1007/s00382-019-04645-z.

Li, Y. J., and J. P. Li, 2012: Propagation of planetary waves in the horizontal non-uniform basic flow. *Chinese Journal of Geophysics*, **55**, 361–371, https://doi.org/10.6038/j.issn.0001-5733.2012.02.001. (in Chinese with English abstract)

Li, Y. J., J. P. Li, F.-F. Jin, and S. Zhao, 2015: Interhemispheric propagation of stationary Rossby waves in a horizontally nonuniform background flow. *J. Atmos. Sci.*, **72**, 3233–3256, https://doi.org/10.1175/JAS-D-14-0239.1.

Li, Y. J., J. Feng, J. P. Li, and A. X. Hu, 2019b: Equatorial windows and barriers for stationary Rossby wave propagation. *J. Climate*, **32**, 6117–6135, https://doi.org/10.1175/JCLI-D-18-0722.1.

Liu, T., J. P. Li, and F. Zheng, 2015: Influence of the boreal autumn southern annular mode on winter precipitation over land in the Northern Hemisphere. *J. Climate*, **28**, 8825–8839, https://doi.org/10.1175/JCLI-D-14-00704.1.

Luo, D. H., Y. N. Chen, A. G. Dai, M. Mu, R. H. Zhang, and S. Ian, 2017: Winter Eurasian cooling linked with the Atlantic Multidecadal Oscillation. *Environmental Research Letters*, **12**, 125002, https://doi.org/10.1088/1748-9326/aa8de8.

Luo, F. F., and S. L. Li, 2014: Joint statistical-dynamical approach to decadal prediction of East Asian surface air temperature. *Science China Earth Sciences*, **57**, 3062–3072, https://doi.org/10.1007/s11430-014-4984-3.

Meehl, G. A., and H. Y. Teng, 2014: CMIP5 multi-model hindcasts for the mid-1970s shift and early 2000s hiatus and predictions for 2016–2035. *Geophys. Res. Lett.*, **41**, 1711–1716, https://doi.org/10.1002/2014GL059256.

Meehl, G. A., H. Y. Teng, and J. M. Arblaster, 2014: Climate model simulations of the observed early-2000s hiatus of global warming. *Nature Climate Change*, **4**, 898–902, https://doi.org/10.1038/nclimate2357.

Morice, C. P., J. J. Kennedy, N. A. Rayner, and P. D. Jones, 2012: Quantifying uncertainties in global and regional temperature change using an ensemble of observational estimates: The HadCRUT4 data set. *J. Geophys. Res.: Atmos.*, **117**, D08101, https://doi.org/10.1029/2011jd017187.

Nigam, S., A. Sengupta, and A. Ruiz-Barradas, 2020: Atlantic-Pacific links in observed multidecadal SST variability: Is the Atlantic Multidecadal Oscillation's phase reversal orchestrated by the Pacific Decadal Oscillation? *J. Climate*, **33**, 5479–5505, https://doi.org/10.1175/JCLI-D-19-0880.1.

Pyper, B. J., and R. M. Peterman, 1998: Comparison of methods to account for autocorrelation in correlation analyses of fish data. *Canadian Journal of Fisheries and Aquatic Sciences*, **55**, 2127–2140, https://doi.org/10.1139/cjfas-55-12-2710.

Rayner, N. A., D. E. Parker, E. B. Horton, C. K. Folland, L. V. Alexander, D. P. Rowell, E. C. Kent, and A. Kaplan, 2003: Global analyses of sea surface temperature, sea ice, and night marine air temperature since the late nineteenth century. *J. Geophys. Res.*, **108**, 4407, https://doi.org/10.1029/2002JD002670.

Schlesinger, M. E., and N. Ramankutty, 1994: An oscillation in the global climate system of period 65–70 years. *Nature*,

367(6465), 723–726, https://doi.org/10.1038/367723a0.

Stolpe, M. B., I. Medhaug, J. Sedláček, and R. Knutti, 2018: Multidecadal variability in global surface temperatures related to the Atlantic Meridional Overturning Circulation. *J. Climate*, **31**(7), 2889–2906, https://doi.org/10.1175/JCLI-D-17-0444.1.

Sun, C., and J. P. Li, 2012: Analysis of anomalously low surface air temperature in the Northern Hemisphere during 2009/2010 winter. *Climatic and Environmental Research*, **17**, 259–273, https://doi.org/10.3878/j.issn.1006-9585.2011.10070. (in Chinese with English abstract)

Sun, C., J. P. Li, and F.-F. Jin, 2015: A delayed oscillator model for the quasi-periodic multidecadal variability of the NAO. *Climate Dyn.*, **45**, 2083–2099, https://doi.org/10.1007/s00382-014-2459-z.

Sun, C., J. P. Li, R. Q. Ding, and Z. Jin, 2017a: Cold season Africa-Asia multidecadal teleconnection pattern and its relation to the Atlantic multidecadal variability. *Climate Dyn.*, **48**, 3903–3918, https://doi.org/10.1007/s00382-016-3309-y.

Sun, C., J. P. Li, F. Kucharski, J. Q. Xue, and X. Li, 2019: Contrasting spatial structures of Atlantic Multidecadal Oscillation between observations and slab ocean model simulations. *Climate Dyn.*, **52**, 1395–1411, https://doi.org/10.1007/s00382-018-4201-8.

Sun, C., F. Kucharski, J. P. Li, F.-F. Jin, I.-S. Kang, and R. Q. Ding, 2017b: Western tropical Pacific multidecadal variability forced by the Atlantic multidecadal oscillation. *Nature Communications*, **8**, 15998, https://doi.org/10.1038/ncomms15998.

Sun, J. Q., S. Wu, and J. Ao, 2016: Role of the North Pacific sea surface temperature in the East Asian winter monsoon decadal variability. *Climate Dyn.*, **46**, 3793–3805, https://doi.org/10.1007/s00382-015-2805-9.

Trenberth, K. E., and D. A. Paolino, 1980: The Northern Hemisphere sea-level pressure data set: Trends, errors and discontinuities. *Mon. Wea. Rev.*, **108**(7), 855–872, https://doi.org/10.1175/1520-0493(1980)108<0855:TNHSLP>2.0.CO;2.

University of East Anglia Climatic Research Unit, I. C. Harris, and P. D. Jones, 2017: CRU TS4.01: Climatic Research Unit (CRU) Time-Series (TS) version 4.01 of high-resolution gridded data of month-by-month variation in climate (Jan. 1901-Dec. 2016). Centre for Environmental Data Analysis, http://dx.doi.org/10.5285/58a8802721c94c66ae45c3baa4d814d0.

von Storch, H., and F. W. Zwiers, 2002: *Statistical Analysis in Climate Research*. Cambridge University Press, 162 pp.

Wallace, J. M., Y. Zhang, and L. Bajuk, 1996: Interpretation of interdecadal trends in Northern Hemisphere surface air temperature. *J. Climate*, **9**(2), 249–259, https://doi.org/10.1175/1520-0442(1996)009<0249:IOITIN>2.0.CO;2.

Wang, B., Z. W. Wu, C. P. Chang, J. Liu, J. P. Li, and T. J. Zhou, 2010: Another Look at interannual-to-interdecadal variations of the East Asian winter monsoon: the northern and southern temperature modes. *J. Climate*, **23**, 1495–1512, https://doi.org/10.1175/2009JCLI3243.1.

Wang, L., and W. Chen, 2010: Downward Arctic Oscillation signal associated with moderate weak stratospheric polar vortex and the cold December 2009. *Geophys. Res. Lett.*, **37**, L09707, https://doi.org/10.1029/2010GL042659.

Wang, L., and W. Chen, 2014a: The East Asian winter monsoon: Re-amplification in the mid-2000s. *Chinese Science Bulletin*, **59**, 430–436, https://doi.org/10.1007/s11434-013-0029-0.

Wang, L., and W. Chen, 2014b: A CMIP5 multimodel projection of future temperature, precipitation, and climatological drought in China. *International Journal of Climatology*, **34**(6), 2059–2078, https://doi.org/10.1002/joc.3822.

Wang, X. F., J. P. Li, C. Sun, and T. Liu, 2017: NAO and its relationship with the Northern Hemisphere mean surface temperature in CMIP5 simulations. *J. Geophys. Res.: Atmos.*, **122**(8), 4202–4227, https://doi.org/10.1002/2016JD025979.

Wills, R. C. J., K. C. Armour, D. S. Battisti, and D. L. Hartmann, 2019: Ocean-atmosphere dynamical coupling fundamental to the Atlantic Multidecadal Oscillation. *J. Climate.*, **32**, 251–272, https://doi.org/10.1175/JCLI-D-18-0269.1.

Wu, B. Y., and J. Wang, 2002: Winter arctic oscillation, Siberian high and East Asian winter monsoon. *Geophys. Res. Lett.*, **29**(19), 1897, https://doi.org/10.1029/2002gl015373.

Wu, B. Y., J. Z. Su, and R. H. Zhang, 2011a: Effects of autumn-winter arctic sea ice on winter Siberian high. *Chinese Science Bulletin*, **56**, 3220–3228, https://doi.org/10.1007/s11434-011-4696-4.

Wu, Z. W., J. Dou, and H. Lin, 2015: Potential influence of the November-December Southern Hemisphere annular mode on the East Asian winter precipitation: A new mechanism. *Climate Dyn.*, **44**, 1215–1226, https://doi.org/10.1007/s00382-014-2241-2.

Wu, Z. W., J. P. Li, B. Wang, and X. H. Liu, 2009: Can the Southern Hemisphere annular mode affect China winter monsoon? *J. Geophys. Res.*, **114**, D11107, https://doi.org/10.1029/2008JD011501.

Wu, Z. W., J. P. Li, Z. H. Jiang, and J. H. He, 2011b: Predictable climate dynamics of abnormal East Asian winter monsoon: Once-in-a-century snowstorms in 2007/2008 winter. *Climate Dyn.*, **37**, 1661–1669, https://doi.org/10.1007/s00382-010-0938-4.

Xie, T. J., J. P. Li, K. Q. Chen, Y. Z. Zhang, and C. Sun, 2021: Origin of Indian Ocean multidecadal climate variability: Role of the North Atlantic Oscillation. *Climate Dyn.*, **56**, 3277–3294, https://doi.org/10.1007/s00382-021-05643-w.

Xie, T. J., J. P. Li, C. Sun, R. Q. Ding, K. C. Wang, C. F. Zhao, and J. Feng, 2019: NAO implicated as a predictor of the surface air temperature multidecadal variability over East Asia. *Climate Dyn.*, **53**, 895–905, https://doi.org/10.1007/s00382-019-04624-4.

Xing, N., J. P. Li, and L. N. Wang, 2017: Multidecadal trends in large-scale annual mean SATa based on CMIP5 historical simulations and future projections. *Engineering*, **3**, 136–143, https://doi.org/10.1016/J.ENG.2016.04.011.

Xu, Y. D., and Coauthors, 2020: Contribution of SST change to multidecadal global and continental surface air temperature trends between 1910 and 2013. *Climate Dyn.*, **54**, 1295–1313, https://doi.org/10.1007/s00382-019-05060-0.

Yin, S., J. Feng, and J. P. Li, 2013: Influences of the preceding winter Northern Hemisphere annular mode on the spring extreme low temperature events in the north of eastern China. *Acta Meteorologica Sinica*, **71**(1), 96–108, https://doi.org/10.11676/qxxb2013.008.(inChinesewithEnglishabstract). (in Chinese with English abstract)

Yu, L. L., Z. W. Wu, R. H. Zhang, and X. Yang, 2018: Partial least regression approach to forecast the East Asian winter monsoon using Eurasian snow cover and sea surface temperature. *Climate Dyn.*, **51**(11), 4573–4584, https://doi.org/10.1007/s00382-017-3757-z.

Yun, K.-S., Y.-W. Seo, K.-J. Ha, J.-Y. Lee, and Y. Kajikawa, 2014: Interdecadal changes in the Asian winter monsoon variability and its relationship with ENSO and AO. *Asia-Pacific Journal of Atmospheric Sciences*, **50**(4), 531–540, https://doi.org/10.1007/s13143-014-0042-5.

Zhang, P., Z. W. Wu, and J. P. Li, 2019: Reexamining the relationship of La Niña and the East Asian winter monsoon. *Climate Dyn.*, **53**, 779–791, https://doi.org/10.1007/s00382-019-04613-7.

Zhang, P., Z. W. Wu, J. P. Li, and Z. N. Xiao, 2020: Seasonal prediction of the northern and southern temperature modes of the East Asian winter monsoon: The importance of the Arctic sea ice. *Climate Dyn.*, **54**, 3583–3597, https://doi.org/10.1007/s00382-020-05182-w.

Zhao, P., P. Jones, L. Cao, Z. Yan, S. Zha, Y. Zhu, Y. Yu, and G. Tang, 2014: Trend of surface air temperature in Eastern China and associated large-scale climate variability over the last 100 years. *J. Climate*, **27**(12), 4693–4703, https://doi.org/10.1175/JCLI-D-13-00397.1.

Zhao, S., J. P. Li, and Y. J. Li, 2015: Dynamics of an interhemispheric teleconnection across the critical latitude through a southerly duct during boreal winter. *J. Climate*, **28**, 7437–7456, https://doi.org/10.1175/JCLI-D-14-00425.1.

Zhao, S., J. P. Li, Y. J. Li, F.-F. Jin, and J. Y. Zheng, 2019: Interhemispheric influence of Indo-Pacific convection oscillation on Southern Hemisphere rainfall through southward propagation of Rossby waves. *Climate Dyn.*, **52**, 3203–3221, https://doi.org/10.1007/s00382-018-4324-y.

Zheng, F., J. P. Li, and T. Liu, 2014: Some advances in studies of the climatic impacts of the Southern Hemisphere annular mode. *J. Meteor. Res.*, **28**(5), 820–835, https://doi.org/10.1007/s13351-014-4079-2.

Zheng, F., J. P. Li, L. Wang, F. Xie, and X. F. Li, 2015: Cross-seasonal influence of the December–February Southern Hemisphere annular mode on March–May meridional circulation and precipitation. *J. Climate*, **28**, 6859–6881, https://doi.org/10.1175/JCLI-D-14-00515.1.

Zheng, F., and Coauthors, 2021: The 2020/21 extremely cold winter in China influenced by the synergistic effect of La Niña and warm Arctic. *Adv. Atmos. Sci.*, https://doi.org/10.1007/s00376-021-1033-y

Zuo, B., J. P. Li, C. Sun, and X. Zhou, 2019: A new statistical method for detecting trend turning. *Theor. Appl. Climatol.*, **138**, 201–213, https://doi.org/10.1007/s00704-019-02817-9.

Zuo, J. Q., H. L. Ren, and W. J. Li, 2015: Contrasting impacts of the Arctic Oscillation on surface air temperature anomalies in southern China between early and middle-to-late winter. *J. Climate*, **28**(10), 4015–4026, https://doi.org/10.1175/JCLI-D-14-00687.1.